https://doi.org/10.5194/egusphere-2026-5278
Preprint. Discussion started: 22 September 2026


# Decadal modulation of ENSO dynamics emerges primarily from white-noise forcing

Jemma Jeffree[1,2], Nicola Maher[1,2], Courtney Quinn[3], and Dietmar Dommenget[4]

[1]Research School of Earth Sciences, Australian National University, Canberra, Australia
[2]ARC Centre of Excellence for 21st Century Weather, Australia
[3]School of Natural Sciences, University of Tasmania, Hobart, Australia
[4]School of Earth and Environment, Monash University, Melbourne, Australia

**Correspondence:** Jemma Jeffree (jemma.jeffree@anu.edu.au)

**Abstract.** Decadal variation in the behaviour of the El Niño Southern Oscillation (ENSO) affects our ability to predict ENSO and to identify its response to climate change. With the aim to better characterise and understand the causes of this decadal modulation of ENSO, we vary the terms of a recharge oscillator model (ROM). We then analyse the resulting decadal variations in Bjerknes index (a measure of growth rate, influencing amplitude) and Wyrtki index (a measure of phase speed, influencing periodicity). These indices are compared across output from ROMs of varying nonlinearity, as well as observations, and output from CMIP models. We find that a linear ROM with stochastic noise forcing explains over 75% of decadal modulation in both observations and a full CMIP model. This creates a null hypothesis against which to compare additional processes to explain ENSO decadal modulation, and highlights the impacts of high-frequency atmospheric noise forcing on ENSO behaviour. Considering our findings that empirically fitted nonlinearities do little to alter ROM representation of ENSO decadal modulation, and full CMIP models exhibit the same timescale of ENSO predictability as a ROM, we suggest that the primary driver of ENSO decadal modulation in Bjerknes index and Wyrtki index is stochastic atmospheric forcing on sub-monthly timescales.

**Plain language summary.** The El Niño Southern Oscillation (ENSO) is characterised by a pattern of warmer or cooler ocean temperatures in the tropical Pacific Ocean, which impacts rain and other weather around the world. Something that has intrigued scientists about ENSO is the way that it seems to behave differently in different decades. For example, during 1990-1999 ENSO events grew more strongly, and switched more slowly between the opposite phases of El Niño and La Niña. In contrast, during 2000-2009 ENSO events were smaller in magnitude and appeared to switch phase faster. In this study we ask what might have caused these decadal changes. We consider a simple linear model (recharge oscillator model) of ENSO with white noise forcing, and find that this is enough to explain more than three quarters of the differences between ENSO behaviour in different decades. Therefore, random weather that changes from month to month (the 'white noise forcing') in the Pacific has more impact than previously suggested for these long decadal timescales.

## 1 Introduction

In recent decades, ENSO has exhibited changes in many characteristics, including amplitude, periodicity, longitude of peak SST anomaly, and predictability (McPhaden, 2012; Barnston et al., 2012; Fang et al., 2019; Pascolini-Campbell et al., 2015;

https://doi.org/10.5194/egusphere-2026-5278
Preprint. Discussion started: 22 September 2026


Hu et al., 2020; Weisheimer et al., 2022). Furthermore, changes have also been observed in ENSO dynamics (Capotondi and Sardeshmukh, 2017; Kim and An, 2020; Crespo et al., 2022). These ENSO changes are a combination of a possible response to climate change and unforced decadal variability (Newman et al., 2011; Borlace et al., 2013; Wittenberg et al., 2014; Dieppois et al., 2021). To distinguish between climate change induced changes in ENSO and it's decadal variability, and thereby interpret observed changes to inform future predictions, it is critical to first understand ENSO decadal variability. This work focuses on the causes of changes in ENSO linear behaviour on decadal timescales. Specifically, we focus on decadal modulation of the defining features of ENSO's oscillation – growth rate and phase speed – as quantified by the Bjerknes and Wyrtki indices respectively (Jin et al., 2006; Lu et al., 2018; Jin et al., 2020; Vialard et al., 2025). This will hereafter be referred to as decadal modulation of ENSO.

The many facets of ENSO decadal variability are interlinked. Decadal changes in ENSO amplitude are associated with changes in the: tropical Pacific mean state (Burgman et al., 2008; Imada and Kimoto, 2009; Choi et al., 2012), longitude of largest amplitude SST anomaly (Choi et al., 2012; Schlör et al., 2024), and ENSO predictability (McPhaden, 2012; Zheng et al., 2016; Fang et al., 2019). Likewise, decadal changes in ENSO, as quantified by amplitude or predictability, can be attributed to changes in ENSO dynamics, such as ENSO growth rate and the thermocline feedback (Zheng et al., 2016; Fang et al., 2019; Kim and Kug, 2022). Decadal changes in ENSO's predictability can also be linked to changes in its dynamical feedbacks. The relationships between all facets of ENSO decadal changes suggest either that they are all controlled by a single driver, or that tightly coupled feedbacks exist between the different aspects of decadal variability. In either case, the strong relationships suggest that identifying causes of one aspect of ENSO decadal variability is nonetheless relevant for many aspects of ENSO decadal variability.

Theories for the origins of decadal variations in ENSO behaviour typically fall under one of three categories: (1) nonlinear dynamics within the equatorial Pacific, (2) additional variables within the equatorial Pacific, or (3) forcing/oscillations external to the equatorial Pacific. Suggestions of the first type highlight that a nonlinear or chaotic system can produce different linear dynamics for different epochs (e.g. Timmermann and Jin, 2002). Of the second type, the most common theory is a key role for changes in the tropical Pacific mean state. According to both model experiments and theoretical arguments, changes in the tropical Pacific mean state modify ENSO asymmetry and amplitude (Sun and Okumura, 2020; Atwood et al., 2017). However, these mean state changes are not caused by ENSO itself and must instead be externally driven because the ENSO response to any mean state change in the tropical Pacific acts to reduce that mean state change (Atwood et al., 2017). External drivers of ENSO decadal changes may include temperature anomalies in other ocean regions, such as the Pacific Decadal Oscillation or Atlantic multi-decadal oscillation (Feng and Tung, 2020; Gong et al., 2020), or temperature-compensated salinity anomalies in the extratropical Pacific (Zeller et al., 2021). For a more detailed description of the various theories for ENSO decadal variability, see Fedorov et al. (2020), Capotondi et al. (2023), and references therein.

To distinguish between different potential causes of ENSO decadal modulations, we compare the ENSO behaviour in observations or a coupled climate model with a conceptual model, where specific dynamics can be included or excluded. The conceptual model of ENSO we use is the recharge oscillator model (ROM): an oscillation arising from feedbacks between sea surface temperature (SST) anomalies and thermocline depth anomalies, and forced by atmospheric white noise (Jin, 1997;

https://doi.org/10.5194/egusphere-2026-5278
Preprint. Discussion started: 22 September 2026


Timmermann et al., 2018; Vialard et al., 2025). Most aspects of ENSO behaviour can be represented within this conceptual framework. For example, ENSO phase locking and the spring predictability barrier can be reproduced with the addition of a seasonally varying growth rate (Levine and McPhaden, 2015; Chen and Jin, 2020, 2021). A positive skewness in ENSO SST index can be achieved via the inclusion of either state-dependent noise forcing (Jin et al., 2007; Levine et al., 2016) or a nonlinear growth-rate of SST anomalies (Dommenget and Al-Ansari, 2023). Recent work with multiple deterministic and stochastic nonlinear terms captures the asymmetry of ENSO SST index and the asymmetry of phase transitions between El Niños and La Niñas (Han et al., 2026). Longitudinal variability in the location of the ENSO anomaly peak (i.e. Central Pacific vs Eastern Pacific El Niños) can be accounted for by changing the SST variable to measure longitudinal shifts (Thual and Dewitte, 2023), or with two SST variables representing different regions of the equatorial Pacific (Chen et al., 2022). The ROM model of ENSO has also been expanded to include bi-directional coupling with SST variables representing climate modes in other basins (Jansen et al., 2009; Zhao et al., 2024), raising ENSO forecast skill to be comparable with forecasts from machine learning models or full coupled GCMs (Zhao et al., 2024). Therefore the ROM offers a good representation of ENSO, and a good framework from which to investigate ENSO decadal variability.

We empirically estimate ROM parameters from both observations and model output. Primarily, the linear parameters from individual decades can be used to quantify decadal modulation of ENSO behaviour, using the Bjerknes and Wyrtki indices. Secondly, we create long-term runs of parameter-fitted ROMs with varying levels of nonlinearity, and likewise quantify ENSO decadal behaviour in the ROM output. This comparison enables us to identify the contributions of linear and nonlinear feedbacks represented in a ROM to ENSO decadal modulation in observations and CMIP models. Then, additional lines of evidence, from the power spectrum and perfect model predictability of a ROM versus a coupled climate model, are also used to constrain the origins of ENSO decadal variability.

## 2 Data and Methods

### 2.1 Data

We evaluate ENSO behaviour both in the observational record and in multiple CMIP-class models. The advantages and disadvantages of each dataset are as follows: ENSO dynamics are more realistically represented in observations than in CMIP models. Conversely, the CMIP models provide a larger sample size that enables a more thorough statistical analysis than historical observations. To minimise the effect of any individual models bias on our conclusions, we repeat our analysis across multiple models. Three models are chosen to represent a spread of ENSO asymmetry, which has been linked to how models represent ENSO decadal variability (Kohyama et al., 2017) and cover the CMIP model spread (ACCESS-ESM1-5 is negatively skewed, CanESM5 positively skewed and CESM1-CAM5 strongly positively skewed to the same extend as observations; details in Appendix A and Figure A1).

In the main text, we use the following data sources:

– ORAS5 (observational reanalysis; Copernicus Climate Change Service, 2021)

https://doi.org/10.5194/egusphere-2026-5278
Preprint. Discussion started: 22 September 2026


- ACCESS-ESM1.5 (CMIP6 model; Ziehn et al., 2020)
- CanESM5 (CMIP6 model; Swart et al., 2019; Sospedra-Alfonso et al., 2021)
- CESM1-CAM5 (CMIP5 model; Kay et al., 2015; Yeager et al., 2018)

Additional datasets are shown in the Appendix, with results from additional models supporting the same conclusions as our three chosen models (Compare Figures 3, 4, 5 with Figures D2, D5, D6).

The observations consist of a 40 year record from 1984-2024. This range extends from the first year where there was a physical mooring present in the tropical Pacific (McPhaden, 1993), at which time the ORAS5 reanalysis shows a step-change in thermocline depth (Figure D1), through four complete decades of observed ENSO decadal modulation. The three CMIP models are large ensembles: repetitions of the same model run differing only in initial condition, with 25-50 ensemble members. We use the historical runs from 10 years after initialisation (i.e. 1860 or 1930) through to the last decade of the historical forcing period (2000 or 2010 for CMIP5 or CMIP6 respectively). Both observations and model output are quadratically detrended. This leads to several thousand (2,800 – 5,600) years of output for each model. We also use decadal prediction ensembles from these models (details in Section 2.5).

### 2.2 Recharge Oscillator Model (ROM)

The ROM represents ENSO as two variables: eastern equatorial Pacific SST ($T$) and equatorial Pacific thermocline depth ($h$) (Vialard et al., 2025) (Figure 1). The time-evolution of these variables is controlled by both their values and white noise added to account for the influence of stochastic atmospheric behaviour:

$$\frac{\mathrm{d}T}{\mathrm{d}t} = RT + F_1 h + \sigma_T \xi_T, \tag{1a}$$

$$\frac{\mathrm{d}h}{\mathrm{d}t} = -\varepsilon h - F_2 T + \sigma_h \xi_h. \tag{1b}$$

The parameters $R, \varepsilon, F_1, F_2$ are constants, and $\xi_T, \xi_h$ are Gaussian white noise with variance of 1, modulated by constants $\sigma_T and \sigma_h$ which represent standard deviations of noise forcing. Together, these two equations define the oscillatory behaviour of ENSO.

We define $T$ as the average SST in the NINO34 region. We define $h$ as the average 20 degree isotherm depth across the entire equatorial Pacific (120-280°E), between 5°S-5°N. Both $T$ and $h$ are monthly-averaged anomalies. While the use of other regions or variables has been proposed to calculate either $T$ or $h$ (e.g Izumo et al., 2019; Dommenget et al., 2023; Priya and Dommenget, 2025), the choice of region does not alter our primary result (compare Figures 3 and D2 with Figures D3, D4). A common aim of variable choices in these previous studies is to minimise the correlation between $T$ and $h$ at lag 0, which does not apply to our analysis of Bjerknes and Wyrtki indices (see Appendix B). We note that some later sections of this work do explore the impact of different regions for the $T$ or $h$ variables of the ROM, and in these instances, the departure from the main methods of the paper is specified.

We estimate the ROM parameters $R, \varepsilon, F_1, F_2$ with a multivariate linear regression (Figure 1a, b). For this linear regression, and for later integration of the ROM, we define the tendencies of $T$ and $h$ ($\frac{dT}{dt}$ and $\frac{dh}{dt}$) as the difference between two sequential

https://doi.org/10.5194/egusphere-2026-5278
Preprint. Discussion started: 22 September 2026


monthly averages. In other words, these quantities represent the change from the month of $T$ and $h$ to the next month (Details and justification in Appendix C). We note that the monthly timestep definition of tendency differs from previous work defining these tendencies as a continuous derivative (e.g. Vijayeta and Dommenget, 2018). Nonetheless, we retain conventional notation of differential equation for consistency with existing literature. The standard deviation of white noise forcing $(\sigma_T, \sigma_h)$ is estimated as the standard deviation of the residual to one-month forecasts from the fitted model.

In order to explore how nonlinearities in ENSO contribute to decadal modulation of ENSO behaviour, we consider two additional ROMs that incorporate nonlinear ENSO behaviour. We run these nonlinear ROMs, alongside the linear ROM, to compare the output with observations and CMIP model output. There are many suggestions of how to incorporate ENSO nonlinearity in a ROM (e.g. Takahashi et al., 2019; Kim and An, 2020; Dommenget and Al-Ansari, 2023; Vialard et al., 2025; Han et al., 2026). The specific representation of nonlinearity is important, because an incorrect choice of nonlinear term can misrepresent the behaviour of the system (Weeks and Tziperman, 2025). Instead of systematically evaluating all possible nonlinear models, we consider two models at the opposite ends of the spectrum: a simple quadratic nonlinear model and generic nonlinear model, which can capture any type or magnitude of nonlinearity. The quadratic nonlinear model adds one term to the linear ROM, so that the temperature tendency is quadratically dependent on temperature (as per Vialard et al., 2025):

$$\frac{\mathrm{d}T}{\mathrm{d}t} = RT + F_1 h + bT^2 + \sigma_T \xi_T, \tag{2a}$$
$$\frac{\mathrm{d}h}{\mathrm{d}t} = -\varepsilon h - F_2 T + \sigma_h \xi_h. \tag{2b}$$

This ROM is fitted with a multivariate linear regression as in the linear ROM.

The generic nonlinear ROM is designed to capture the nonlinearity present in large ensembles of CMIP model output, without prior assumptions about the form of these nonlinearities. This differs from the quadratic ROM, where the nonlinearity is specifically represented as a quadratic relationship between $\frac{dT}{dt}$ and $T$. We composite model output into bins of 0.5 standard deviations in $T$ and $h$, and average the tendencies ($\frac{d}{dt}$) in each bin. This produces a 2D field of empirically estimated tendencies for any combination of $T$ and $h$, which is the generic nonlinear ROM (grey arrows, Figure 1b). In equation format, this generic nonlinear ROM is:

$$\frac{\mathrm{d}T}{\mathrm{d}t} = R_T(T,h) + \sigma_T \xi_T, \tag{3a}$$
$$\frac{\mathrm{d}h}{\mathrm{d}t} = R_h(T,h) + \sigma_h \xi_h, \tag{3b}$$

where $R_T(T,h), R_h(T,h)$ are tables of empirically estimated $T$ and $h$ tendencies for a gridded phase space.

Because each bin's tendency is estimated independently, no functional form is imposed on the nonlinearity. The difference when compared to the quadratic ROM can be seen by comparing the grey and red arrows in Figure 1b. Averaging over a large ensemble allows the deterministic aspect of ENSO behaviour to be separated from the stochastic. Bins that have minimal model output (fewer than 5 data points) are replaced with the linear ROM's tendency from the centre of that bin when integrating the ROM. Stochastic noise forcing is included in this ROM, in the same way as in the linear and quadratic ROMs.

https://doi.org/10.5194/egusphere-2026-5278
Preprint. Discussion started: 22 September 2026


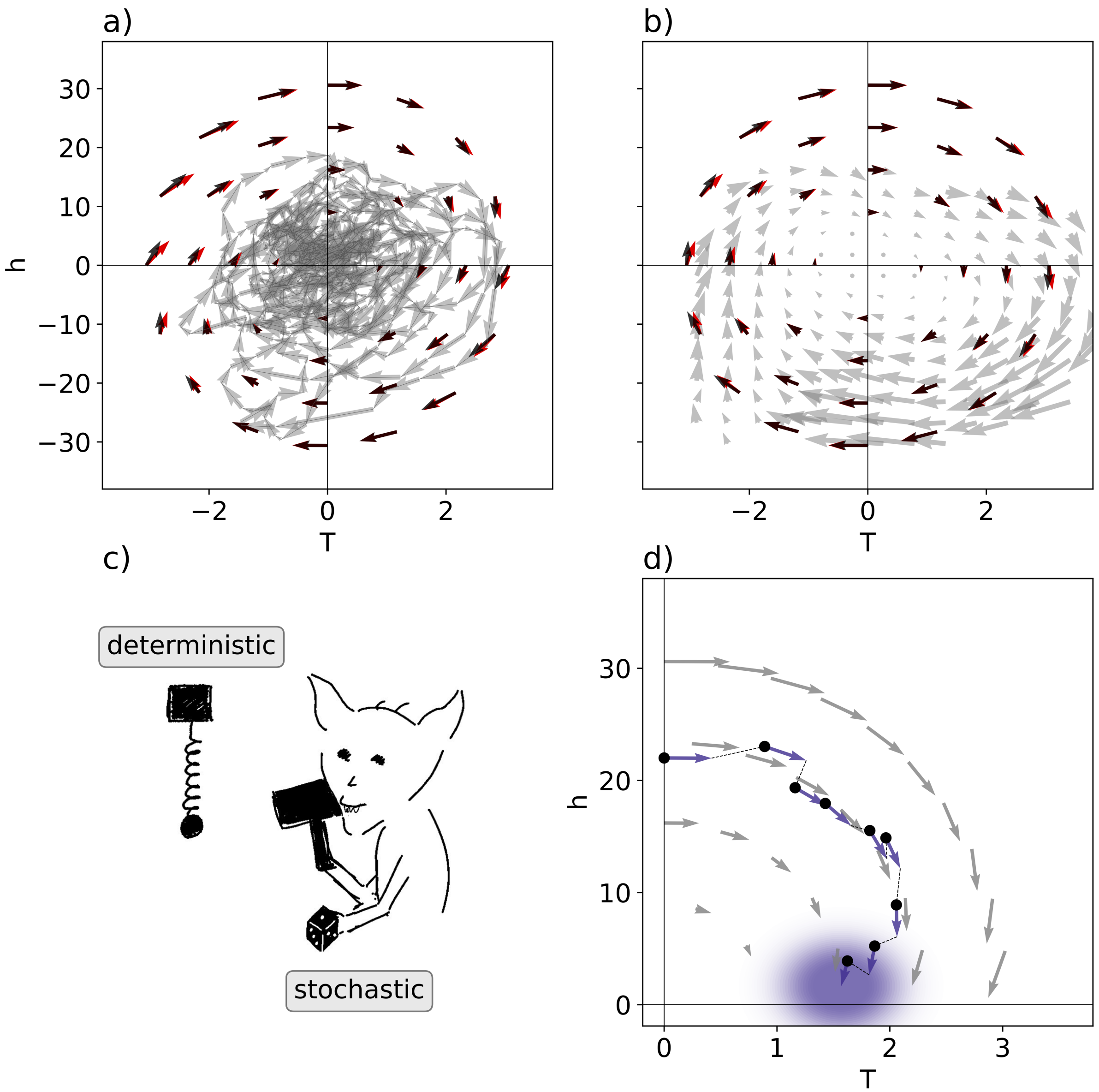


**Figure 1.** Schematic of how the ROM condenses the complex time-evolution of ENSO to a combination of a deterministic response to the monthly-averages of $T$ and $h$ and stochastic noise forcing. Panels a,b) show the tendency of a linear ROM (black arrows) and a quadratic ROM (red arrows). In grey, the timeseries of ENSO that was used to fit the ROM: observations (panel a) or the binned average tendency of a large ensemble (CESM1-CAM5, panel b). Conceptually, integrating the ROM consists of a deterministic and stochastic component (panel c). An example integration is given in panel d, using the linear ROM from panel a (shown in background with grey arrows). The deterministic component (purple arrows) and stochastic component (dashed lines or shaded purple for final arrow) together contribute to the trajectory of modelled ENSO, moving from one black dot to the next.

https://doi.org/10.5194/egusphere-2026-5278
Preprint. Discussion started: 22 September 2026


### 2.3 Producing ROM timeseries

We numerically integrate these three ROMs (linear, quadratic and generic) to produce output for comparison with observations and CMIP models. The ROM consists of both deterministic and stochastic processes, and so to produce a ROM timeseries we model both of these (Figure 1c, d). The deterministic component produces a damped oscillation. The stochastic component, representing faster-timescale processes, leads to deviations from this predictable oscillation.

To produce simulated ROM runs, we calculate the monthly tendency of $T$ and $h$ from the ROM, add that to the current $T$ and $h$, and then add a single instance of white Gaussian noise (details in Appendix C). We then repeat this process for the additional months of each simulation. To compare with CMIP large ensembles, ROM timeseries were created for 100 ensemble members with a run length of 3720 months, for which the first 120 months were discarded to remove dependence on initialisation. This produces 30,000 years of ROM output per run.

### 2.4 Analysis

Parameter estimates from the empirically fitted linear ROM underpin the indices we use to understand ENSO behaviour: the Bjerknes index and Wyrtki index (Jin et al., 2006; Lu et al., 2018; Jin et al., 2020; Vialard et al., 2025). The Bjerknes index represents the rate at which an anomaly in the ENSO *system* (i.e., both $T$ and $h$) grows or decays over time, while the Wyrtki index represents the rate at which an anomaly in the ENSO system changes phase (moves between anomalies of $T$ and $h$, and consequently between positive and negative $T$). These indices can be calculated with the following formulae:

$$\text{Bjerknes index} = \frac{R-\varepsilon}{2} \tag{4a}$$

$$\text{Wyrtki index} = \frac{1}{2}\sqrt{4F_1F_2-(R+\varepsilon)^2} \tag{4b}$$

which are equivalent to the real and imaginary components of the eigenvalues of Equation 1.

By comparing the Bjerknes and Wyrtki indices from the observations or full GCMs with both linear and nonlinear ROMs, we can apportion decadal variation in ENSO linear dynamics to the processes represented in these different models.

### 2.5 Initialised ensembles to estimate predictability

This initial analysis leads us to ask what processes are residuals to ROM fits, and are represented in the ROM as noise. To identify the timescale of these processes, we quantify perfect model predictability in CMIP models and compare it to perfect model predictability in a ROM. Perfect model predictability is the inherent predictability of a model forecasting itself, and can be used to measure predictability limits from internal variability unaffected by model biases. For this purpose, we primarily use existing simulations from the Decadal Climate Prediction Project (DCPP) CMIP collection, which consist of 58+ initialisations with 10+ ensemble members, run for 10 years each (Boer et al., 2016). Models in the main text from this collection (CanESM5, CESM1-CAM5) are initialised in November.

https://doi.org/10.5194/egusphere-2026-5278
Preprint. Discussion started: 22 September 2026


We also ran a new initialised ensemble of ACCESS-ESM1-5 with pre-industrial forcing (Ziehn et al., 2020), designed to estimate predictability from initialisation without the confounding influence of external forcing. The model was initialised from 20 initial conditions, from January every 5 years during a pre-industrial control run. These were perturbed with a magnitude of $10^{-4}$ perturbation to atmospheric temperature for 10 ensemble members, and each was run for 6 years, still with pre-industrial forcing. We compare each initialised ensemble with a ROM run with the same format – the same number of ensemble members and initialisations – and repeat this process 100 times for a bootstrapped spread of expected perfect model predictability.

## 3 Results

### 3.1 ENSO decadal modulation

Changes in ENSO behaviour are visible in the observed timeseries of NINO34 SST anomalies (Figure 2a). For example, the decade 2000-2009 (black outline in Figure 2a) was characterised by a smaller ENSO amplitude and shorter ENSO period, leading to poor ENSO predictability (Barnston et al., 2012; McPhaden, 2012; Lübbecke and McPhaden, 2014). This decadal modulation of ENSO may be quantified using the Bjerknes and Wyrtki indices (ENSO growth rate and phase speed respectively; see Figures 2b,c). In the aforementioned decade 2000-2009, the smaller amplitude of ENSO events is reflected in the more negative Bjerknes index (faster decay of ENSO anomalies) and the shorter ENSO period is reflected in the the larger Wyrtki index (faster phase changes) over this period (see square marker in Figures 2b,c).

To establish a baseline decadal modulation from stochastic forcing, we fit a linear ROM to observations, and run it for 3000 decades. We calculate the Bjerknes and Wyrtki indices in each decade of ROM output (Figure 3)a,b. The resulting spread of decades from the linear ROM indicates the spread in decadal modulation we would expect from stochastic forcing, with no underlying change in parameters. This spread encompasses the four sequential decades from observations (compare vertical lines with black outline in Figure 3a,b; p>0.05). In other words, the observed decadal modulation is not statistically different from a linear ROM with white noise forcing, although the linear ROM has no change in the underlying parameters. Therefore, the behaviour of $T$ and $h$ during the observational record does not support the argument that decadal ENSO modulation is caused by any terms omitted from the linear ROM.

By construction, the linear ROM's dynamical parameters remain constant across all decades of model output. The only difference between decades is the white noise forcing. Therefore, the spread in estimated Bjerknes and Wyrtki indices of the linear ROM must originate from this noise, not from changes in the underlying dynamics. The fact that this spread aligns with observations suggests that a process modelled as noise can be responsible for the observed variability in the Bjerknes and Wyrtki indices. We illustrate this with a hypothetical decade. Suppose, in this decade, the white noise added to $T$ by chance correlates strongly with $T$ itself. When we estimate the parameter $R$ (which links $T$ and $\frac{dT}{dt}$) from this decade's timeseries of $T$ and $h$, the estimation procedure captures a combination of the true dynamical relationship and the correlated noise and thereby produces an inflated value of $R$. This also produces a larger estimate of Bjerknes index, even though the ROM's true underlying Bjerknes index hasn't changed. Meanwhile, the same correlated noise directly amplifies ENSO by growing anomalies when they are already large, producing a higher decadal amplitude. More generally, this implies that a link between an emergent

https://doi.org/10.5194/egusphere-2026-5278
Preprint. Discussion started: 22 September 2026


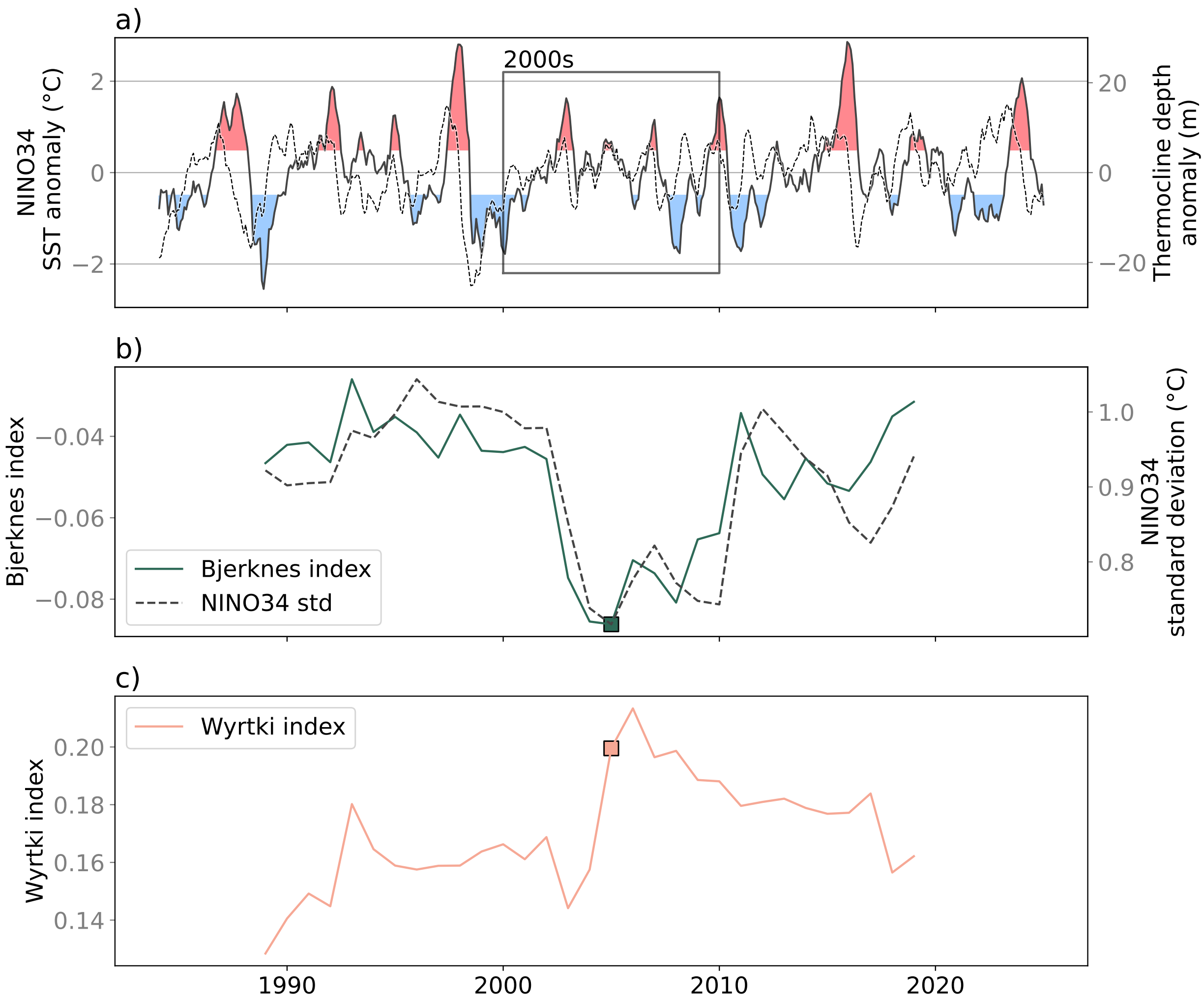


**Figure 2.** Observed decadal variability in ENSO. a) Timeseries of observed NINO34 ($T$) and thermocline depth ($h$) anomaly. b) Bjerknes index in a 10yr sliding window (green), and ENSO amplitude as estimated by the standard deviation of $T$ in a 10yr sliding window. These two metrics are correlated (r=0.80) c) Wyrtki index of ENSO periodicity in a 10yr sliding window. The 2000s (2000-2009 inclusive) are outlined in black in a and marked with a square in b and c.

https://doi.org/10.5194/egusphere-2026-5278
Preprint. Discussion started: 22 September 2026


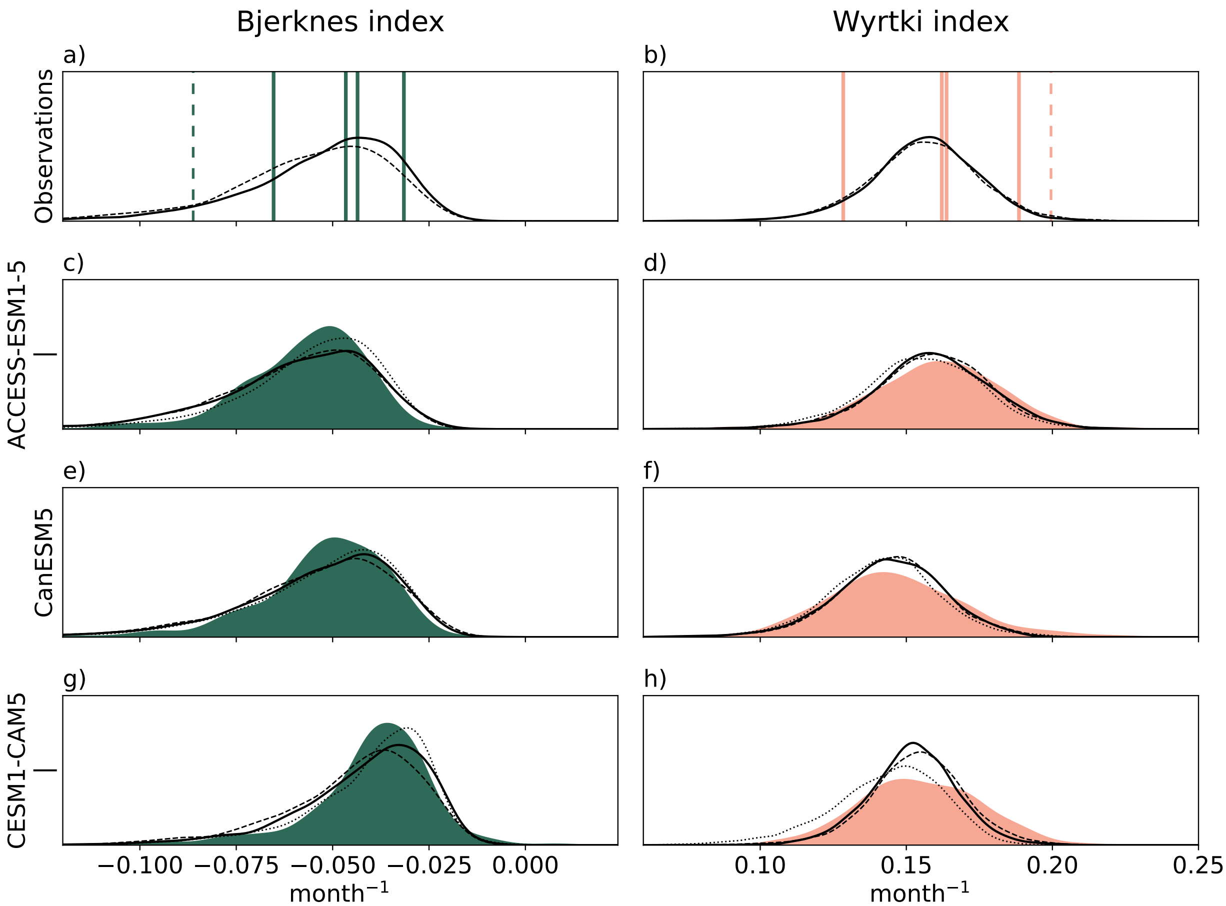


**Figure 3.** Spread of decadal behaviour in ENSO, in observations (a-b, vertical lines) and CMIP-class models (c-f, coloured distribution) as compared to a recharge oscillator model (ROM) with linear parameters (solid line), quadratic parameters (dashed line), or a generic nonlinear approach (dotted line). All distributions are calculated using kernel density estimation. The observations are not statistically different from either ROM (Kolmogorov–Smirnov test, p>0.05), even if the extreme 2000-2009 decade (dashed vertical line) is included in the statistical test as a 5th sample. The CMIP model distributions also show substantial overlap with ROM distributions, although the large sample size means they are statistically different (details in Table 1).

characteristic (e.g. amplitude) and an estimated dynamical term (e.g. Bjerknes index) may not be enough to argue causality, even if there exists a physically logical argument why that dynamical term should affect the emergent characteristic.

We repeat the same analysis with the larger sample size offered by large ensembles of CMIP class models. Figures 3c-f compare decadal modulation from the full CMIP model (coloured distribution) with the linear ROM fitted to that large ensemble (solid black line). Most (77-93%) of the decadal modulation in the large ensemble is explained by the combination of white noise forcing and the linear ROM (Table 1). The addition of quadratic terms (dashed line in Figure 3) or a generic

https://doi.org/10.5194/egusphere-2026-5278
Preprint. Discussion started: 22 September 2026


| | overlap in Bjerknes Index | | | overlap in Wyrtki Index | | |
|---|---|---|---|---|---|---|
| Model | linear | quadratic | generic nonlinear | linear | quadratic | generic nonlinear |
| ACCESS-ESM1-5 | **0.88** | **0.88** | **0.90** | **0.93** | **0.93** | **0.89** |
| CanESM5 | **0.89** | **0.87** | **0.90** | **0.89** | **0.88** | **0.88** |
| CESM1-CAM5 | **0.89** | **0.86** | 0.91 | **0.82** | **0.85** | **0.80** |
| CESM2 | **0.79** | **0.78** | **0.85** | **0.84** | **0.84** | **0.84** |
| IPSL-CM6A-LR | **0.77** | **0.77** | **0.81** | **0.89** | **0.91** | **0.87** |
| MIROC6 | **0.91** | **0.85** | **0.91** | **0.90** | **0.91** | **0.90** |

**Table 1.** Fractional overlap between CMIP large ensemble distribution of Wyrtki/Bjerknes index and ROM fitted to that large ensemble. Bold indicates where a there is a significant difference between the distributions (Kolmogorov–Smirnov test $p<0.05$). The difference between the distributions is almost universally statistically significant with these sample sizes, but $>75\%$ of the distribution is nonetheless captured by the ROM.

nonlinear ROM (dotted line in Figure 3) does not change how well the ROM captures decadal modulation of ENSO. We conclude that, in both climate models and observations, the majority of decadal modulation of ENSO is aligned with that produced by white noise forcing in a linear ROM.

These results are consistent with the Han et al. (under review), who found that the variation in ROM parameters seen in observations is consistent with that produced by a ROM without external forcing. Han et al. (under review) show that the magnitude of these variations from white noise forcing obfuscate any trends or climate change signal. Our results build on and strengthen their conclusions using large ensembles, by showing that most of the internal variability in CMIP model output is also captured by a linear ROM with white noise forcing. Conversely, Capotondi and Sardeshmukh (2017) argue that there are other processes in addition to noise that have impacted observed linear dynamics in the tropical Pacific on decadal timescales. They find statistically significant changes in the linear dynamics of the tropical Pacific between the two decades before 1977 or after 1978. This result is supported by Crespo et al. (2022) in a ROM framework. The differences between these results and our results could be due to the use of earlier time periods that we removed in our study due to limited observations. They could also be explained by the inclusion of dynamics in the broader Pacific region in the Capotondi and Sardeshmukh (2017) study. Alternatively, the decadal differences not due to noise found in previous work could be the smaller magnitude differences we find in the CMIP model analysis between the ROM and the full distribution (Figure 3c-f; overlap of more the three quarters is most, but not all of the distribution).

### 3.2 ENSO power spectrum

Changes in the mean state of the tropical Pacific are often causally linked to changes in ENSO dynamics (Atwood et al., 2017; Fedorov et al., 2020; Capotondi et al., 2023). Within that framework, we might expect decadal or longer variance in ENSO power spectrum to be linked to decadal modulation of ENSO parameters. Therefore, we quantify the ENSO power spectrum of the different ROMs. Incidentally, this also allows us to investigate how the different ROMs we consider exhibit variance

https://doi.org/10.5194/egusphere-2026-5278
Preprint. Discussion started: 22 September 2026


on different timescales. Both the ROMs and CMIP models show a qualitatively similar power spectrums, with a peak on interannual timescales (Figure 4, top row). However, the frequency of this peak differs between each ROM and CMIP model, and the power on decadal timescales is weaker in each ROM than the CMIP model.

The addition of nonlinearities to the ROM does little to change the power spectrum, consistent with minimal impact from nonlinearities on the decadal modulation in Figure 3. In contrast, changes in how T and h are estimated change the power spectrum much more substantially. For example, a ROM using NINO34 for $T$ and equatorial Pacific thermocline depth for $h$ underestimates ENSO decadal variance. However, replacing $h$ with west Pacific thermocline depth (120°-205° E) results in an overestimation of decadal variance. This shows that differences in ENSO power spectrum between a ROM and CMIP model appear to be primarily driven by the choice of variables used to fit the ROM, rather than a fundamental problem with the ROM's representation of ENSO dynamics, linear or nonlinear.

Decadal power of ENSO is influenced by the location of the $h$ and $T$ variables. Changing the $h$ variable to represent only the western Pacific (120°-205° E) dramatically increases the power of $T$ on decadal timescales (Figure 4, red dashed line, top row, labelled $h = h_w$). This indicates that $h$ in these two regions (the whole equatorial Pacific or western Pacific) interacts differently with $T$ to produce different ENSO behaviour, confirming the results of Izumo et al. (2019) who show that different regions of the Pacific capture different recharge processes and oscillations on different timescales. The regional influence on the power spectrum is additionally highlighted by the result that more western regions of $T$ (e.g. NINO4) show higher power on decadal timescales than more eastern regions (e.g. NINO3) in both ROMs and CMIP models. Therefore, different regions of $T$ and $h$ have different linear feedbacks with each other, which produce a different power spectrum when simulated individually.

The differences between feedbacks in different regions is reinforced by the power spectrum peak of NINO3, NINO34 and NINO4. Although the power of these three indices in a CMIP model all peak at the same frequency, the linear ROM fitted to these different regions of $T$ demonstrate an ENSO peak at different frequencies (Figure 4, bottom row). In a full CMIP model, various $T$ regions are highly correlated and show the same ENSO events. This is unsurprising, because these regions are adjacent and affected by the same basin-wide wind patterns of El Niño and La Niña. On the other hand, the ROMs fitted to these different regions show different peaks in the power spectrum, which indicates that different spatial regions of $T$ contribute different dynamics to the ENSO system (Ren and Wang, 2023), just like the different regions of $h$ (Izumo et al., 2019). In combination with our earlier observation that nonlinear terms do very little to change the shape of ENSO power spectrum, this suggests that differing feedbacks in different regions of the equatorial Pacific contribute more to the shape of ENSO power spectrum than nonlinear feedbacks between the two variables $T$ and $h$.

### 3.3 ENSO timescales of predictability

In Figures 2, 3 and Table 1, we found that the processes modelled as noise in a ROM account for more than three quarters of decadal modulation of ENSO behaviour. We further explore the processes omitted from the ROM that could explain the residual differences, with the aim of focussing future research efforts. We quantify ENSO predictability as "perfect model" predictability: the skill of a model (ROM or CMIP) predicting itself, because the way that the ENSO predictability curve decays over time indicates the relative influence of short or long-timescale processes. Figure 5 shows perfect model predictability of

https://doi.org/10.5194/egusphere-2026-5278
Preprint. Discussion started: 22 September 2026


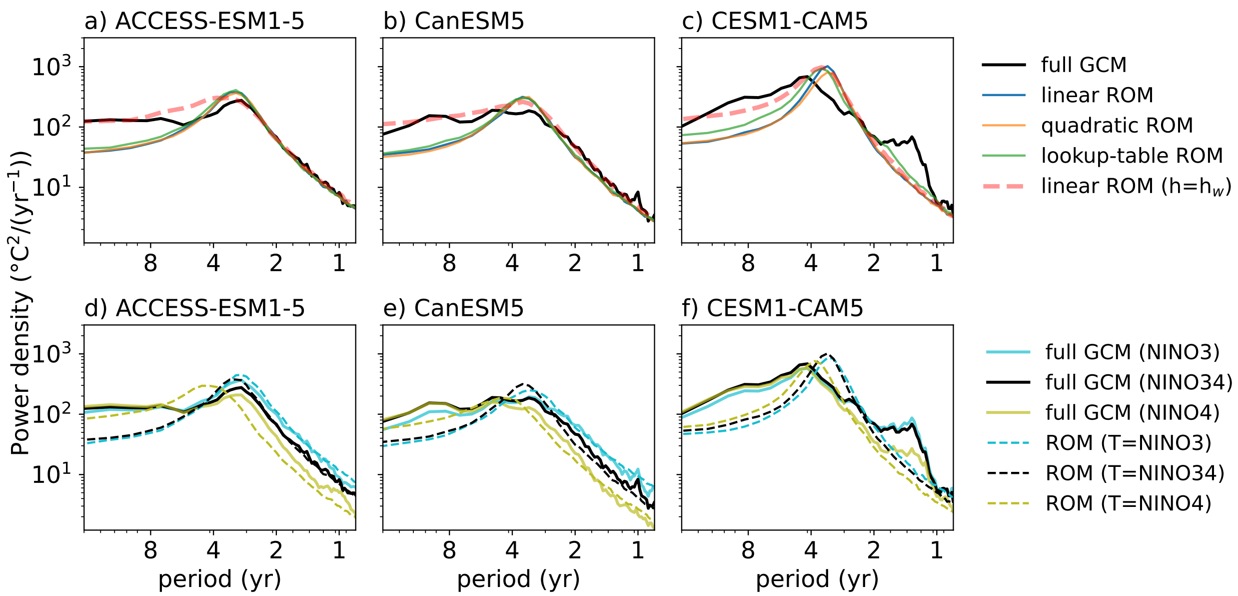


**Figure 4.** Power spectrum of ENSO, as represented by full CMIP models and ROMs. a,b,c) NINO34, with CMIP models in black and various ROMs in colour. d,e,f) CMIP models in faded solid line, and ROMs in dashed line, for different regions of T. We average power spectra from each individual ensemble member in a model. The power spectrum is calculated with Welch's method, with 50 years per segment.

several CMIP models (black lines), which we compare to the perfect-model predictability of a ROM fitted to each CMIP model (purple shading). We use the same experimental setup as the decadal prediction hindcasts from CMIP models (i.e., match the number of initialisations and ensemble members to that specific set of decadal hindcasts), but we repeat the same set of ROM runs 100 times with different stochastic forcing, to give a 95% confidence interval. We also apply the same treatment to uninitialised CMIP large ensembles, to estimate predictability purely from CMIP forcings (e.g., greenhouse gas response, volcanoes; pale blue shading), as the baseline to which we would expect the initialised CMIP models to reach when initialisation provides no further predictability.

In general, the full CMIP model predictabilities (black line) fall within the 95% confidence interval estimated by the ROM (purple shading), until the ROM predictability decays below the predictability of the large ensemble (pale blue shading). At this point, the initialised CMIP model transitions to the same predictability as the uninitialised large ensemble, maintaining some predictability from shared external forcing. However, on interannual to decadal timescales, the ROM demonstrates the same perfect model predictability as an initialised forecast from a CMIP model. The only exception to this is a spike in predictability at 12 months in CanESM5, which likely originates from a strong seasonal cycle in ENSO predictability (i.e. spring predictability barrier, which is known to vary between models (Tian et al., 2019); the ensemble is initialised in November). We would not expect the ROM to capture this seasonal cycle, so it does not affect our main results. Overall, we conclude that processes relevant to ENSO predictability in a CMIP model are of the same timescale as the processes in the ROM (i.e.

https://doi.org/10.5194/egusphere-2026-5278
Preprint. Discussion started: 22 September 2026


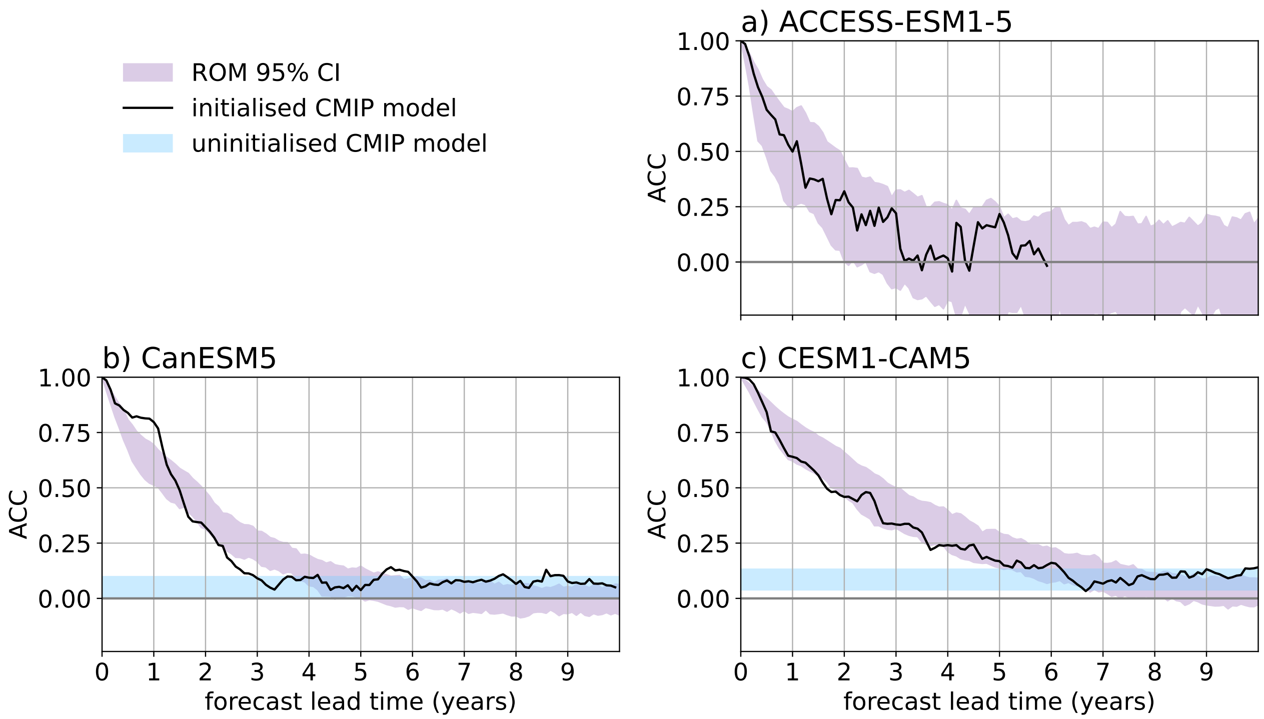


**Figure 5.** Perfect model predictability of ENSO, as quantified by anomaly correlation coefficient (ACC). Purple range shows perfect model predictability of a ROM fitted to a) ACCESS-ESM1-5, b) CanESM5, or c) CESM1-CAM5. Black line indicates the perfect model predictability the full CMIP model. CanESM5 and CESM1-CAM5 were initialised from observations in November each year. A linear trend has been removed to account for some of the climate change forcing, however the predictability of the uninitialised large ensemble for the same time period is added in blue (after detrending) to indicate approximate expected effect of the residual signal. ACCESS-ESM1-5 was run with pre-industrial conditions and initialised from a pre-industrial control run, in January each year, so is expected to have no linear trend or uninitialised predictability.

feedbacks evaluated on a monthly timescale leading to an interannual oscillation), which further implies that CMIP models do not contain decadal timescale processes with a predictable influence on ENSO.

## 4 Discussion

To better understand the processes contributing to ENSO decadal variability, this paper investigates the decadal behaviour of a recharge oscillator model (ROM) of ENSO. We find that the decadal modulation of ENSO in a linear ROM forced by stochastic noise is consistent with the decadal modulation of the observational or CMIP-modelled data to which this ROM was fitted. From this result we draw two conclusions. Firstly, we conclude that atmospheric noise forcing is a key part of ENSO decadal modulation, because the stochastic noise is the only difference between decades in the linear ROM. Secondly, we argue that

https://doi.org/10.5194/egusphere-2026-5278
Preprint. Discussion started: 22 September 2026


dynamical terms omitted from the linear ROM (e.g. nonlinear terms) are not fundamental to ENSO decadal modulation. Both points are expanded in the following paragraphs. Furthermore, we infer that this atmospheric noise forcing can substantially affect estimates of ENSO dynamical terms on decadal timescales, as we see with the Wyrtki and Bjerknes indices here. Some examples of such decadal changes would include the changes in amplitude, period, predictability, and lead/lag relationship between $T$ and $h$ seen after 2000. Therefore, we argue that caution is necessary when considering changes in ENSO behaviour and attributing these behavioural changes to changes in dynamics rather than stochastic atmospheric noise.

We have shown that stochastic noise forcing is sufficient to reproduce the most of ENSO decadal modulation seen in both observations and CMIP models (Figure 3). This implies that processes typically treated as noise can be responsible for decadal changes in ENSO behaviour. In other words, the stochastic contribution to ENSO monthly evolution continues to be important for much longer, decadal, timescales. These processes are not purely high-frequency, but rather processes with a fast decorrelation timescale, including westerly wind events (Capotondi et al., 2018). Understanding these processes is critical for understanding ENSO decadal modulation.

Although a linear ROM with stochastic noise forcing captures most of the expected distribution of ENSO decadal modulation, there remains some difference between the distributions of ENSO decadal modulation in a CMIP model and in a ROM fitted to that CMIP model. Specifically, the ROM overestimates the spread of the Bjerknes index and slightly underestimates the spread of Wyrtki frequency (Figure 3). We recommend future work to understand the origin of these remaining differences in distribution, which we argue likely originate from process of the same short timescale as ROM dynamics or stochastic forcing, because of how we find the ROM represents other aspects of ENSO behaviour on decadal timescales. For example, we find that fully coupled climate models do not show longer timescales of predictability than a ROM (Figure 5), implying that no longer-timescale processes contribute any predictability to a CMIP-modelled ENSO system. Likewise, the variance on decadal timescales of ENSO in CMIP-class models can be replicated in a stochastic linear ROM when considering uncertainty in the location of thermocline feedback (Figure 4), suggesting that no missing dynamics are needed to represent decadal variance in ENSO. We therefore recommend future work to understand the role of sub-monthly forcing of ENSO and sub-monthly ENSO dynamics.

We further argue that these missing short-timescale processes are more likely to be from other state variables such as temperature in other regions in the equatorial or off-equatorial Pacific than from nonlinear processes with the $T$ and $h$ we use here. We find that empirically fitted nonlinearities do not change a ROM's representation of ENSO decadal variability when compared to a linear ROM. Neither the spread of ENSO behaviour in different decades (Figure 3) nor ENSO variance on decadal timescales (Figure 4) are substantially altered by nonlinearities, even if nonlinearities are key to ENSO behaviour as a whole (Han et al., 2026). Our study quantifies ENSO decadal modulation specifically of ENSO linear dynamics, and establishes that this is not strongly affected by nonlinearities.

Furthermore, we find that changing the region used to define variables in a ROM affects decadal variance more than including nonlinearities in the ROM (Figure 4). Likewise, while all three NINO indices peak at the same frequency in a full GCM, a ROM fitted to more western indices (e.g. NINO4) has a lower-frequency peak than a ROM fitted to more eastern indices (e.g. NINO3) (Figure 4). These results suggest that the feedbacks between different regions of the equatorial Pacific make distinct dynamical

https://doi.org/10.5194/egusphere-2026-5278
Preprint. Discussion started: 22 September 2026


contributions to ENSO, which combine to shape the ENSO oscillation. Indices representing ENSO as a longitudinal variation in the background zonal gradient rather than regional averages of SST or thermocline depth (e.g. Williams and Patricola, 2018; Thual and Dewitte, 2023) may therefore better represent ENSO's power spectrum and decadal modulation. More broadly, further research is warranted into the combined role of different Pacific regions – and potentially remote basins – in setting ENSO behaviour across a range of timescales.

Many dynamical processes are omitted from the linear ROM we use in this study. While it is a limitation of this model that it fails to capture the phenomena that depend on these missing processes, we demonstrate that they are not required to reproduce realistic magnitude of decadal modulation of ENSO. For example, the ROM parameters we use do not vary seasonally and are therefore unable to represent ENSO phase locking or a spring predictability barrier. Likewise, the choice of only a single fixed-region SST index limits our ability to represent longitudinal variability in ENSO behaviour. Furthermore, NINO34 variance on decadal timescales from the ROMs does not align with the GCMs to which the ROMs were fitted (Figure 4), and therefore decadal changes in the tropical Pacific mean state are not accurately represented. Despite these limitations, the ROMs presented in this study reproduce over three quarters of the spread of ENSO decadal modulation in CMIP models, originating from stochastic noise forcing. Given that, as argued in the introduction, both ENSO growth rate and many other characteristics of ENSO decadal variation are linked to amplitude changes, the decadal modulation of these characteristics may also be attributable to stochastic noise forcing.

We recognise that biases in CMIP-class models and missing small-scale dynamics may limit the utility of these models for exploring ENSO decadal variability. To minimise the impacts of model-specific biases, we use three separate CMIP models (and an additional four in the appendix), while noting that these models may share common biases. For example, a double-ITCZ bias is present across most of the CMIP5 and CMIP6 ensemble of models (Ren and Zhou, 2024), and many CMIP5 models underestimate pacific SST variance on decadal timescales (Henley et al., 2017). Given that our statistical analysis relies upon large ensemble runs from these CMIP models, because of the short observational record available, these results should be interpreted with caution. If CMIP models under-represent the range of ENSO decadal behaviour modulation, the ROM may accurately reproduce the decadal variability when applied to CMIP, while still underestimating real-world decadal variability.

## 5 Conclusions

We have shown that decadal modulation of ENSO dynamics primarily originates from fast-timescale processes that can be represented by white noise forcing. Our results highlight that to understand ENSO decadal modulation we require a better understanding these fast-timescale processes. We find that the choice of region used to define the variables that represent ENSO in a linear ROM exerts a stronger control on modelled behaviour of ENSO than the addition of nonlinearities to the ROM, highlighting that understanding how variable choice shapes ENSO dynamics is a priority for future research. Overall, we suggest that our original question *"What drives decadal changes in ENSO dynamics?"* should be reframed as *"What drives the processes we model as stochastic noise forcing of ENSO?"* and that future research in this direction is vital for understanding ENSO decadal modulation.

https://doi.org/10.5194/egusphere-2026-5278
Preprint. Discussion started: 22 September 2026


*Code and data availability.* The large ensemble data used in this work is described in Maher et al. (2025) and available from https://rda.ucar.edu/datasets/d651039/ (details https://www.cesm.ucar.edu/community-projects/mmlea/v2). Additional DCPP data is available on the CMIP6 ESGF archive. ORAS5 observational reanalysis data is from Copernicus Climate Change Service (2021)

The code used for analysis is available at https://github.com/jemmajeffree/rom_decadal, and will be moved to zenodo following paper acceptance. Processed data used in the analysis ($T$ and $h$ from large ensemble runs, and $T$ from initialised ensembles) is also available here. The following open-source python packages were key to this analysis: matplotlib (Hunter, 2007), numpy (Harris et al., 2020), scipy (Virtanen et al., 2020), xarray (Hoyer and Hamman, 2017)

## Appendix A: CMIP model choices

We use all models with a large ensemble (>10 members) with sea surface temperature and 20° isotherm depth available as part of Maher et al. (2025), and with a contribution to the Decadal Climate Prediction Project (DCPP) available on gadi (NCI Australia) or glade (NSF NCAR HPC) compute systems. While other modelling groups have potentially run these simulations and have additional data, these models show very similar results. These model runs have between 17 (EC-Earth3) and 50 (CESM2; using only the CMIP6 half of the large ensemble) ensemble members with data available to calculate both $T$ and $h$ throughout the historical simulation, allowing for a large statistical sample size.

| Model name | Large ensemble size | Initialised ensemble size | initialisation | Reference |
|---|---|---|---|---|
| ACCESS-ESM1-5 | 40 | 10 | January 1st | (Ziehn et al., 2020) |
| CanESM5 | 25 | 40 | December 31st | (Swart et al., 2019; Sospedra-Alfonso et al., 2021) |
| CESM1-CAM5 | 39 | 40 | November 1st | (Kay et al., 2015; Yeager et al., 2018) |
| CESM2 | 50 | 20 | November 1st | (Rodgers et al., 2021; Yeager et al., 2022) |
| IPSL-CM6A-LR | 32 | 10 | December 31st | (Boucher et al., 2020; Swingedouw et al., 2026) |
| EC-Earth3 | 17 | 10 | November | (Wyser et al., 2021; Bilbao et al., 2021; Döscher et al., 2022) |
| MIROC6 | 46 | 10 | November 1st | (Tatebe et al., 2019; Kataoka et al., 2020) |

**Table A1.** Models and associated ensemble sizes for the data used in this study

We select three CMIP models for the main text to represent a spread of ENSO asymmetry, as calculated using skewness (Figure A1). The models we use are ACCESS-ESM1-5, CanESM5, and CESM1-CAM5. All three models could feasibly have produced the asymmetry seen in the observational record (though, in the case of ACCESS-ESM1-5, this is on the edge of what is found in the large ensemble), but they have very different mean skewness across the entire large ensemble. ACCESS-ESM1-5 has a negative skewness, CESM1-CAM5 has a positive skewness centred on what is seen in observations, and CanESM5 is in between.

https://doi.org/10.5194/egusphere-2026-5278
Preprint. Discussion started: 22 September 2026


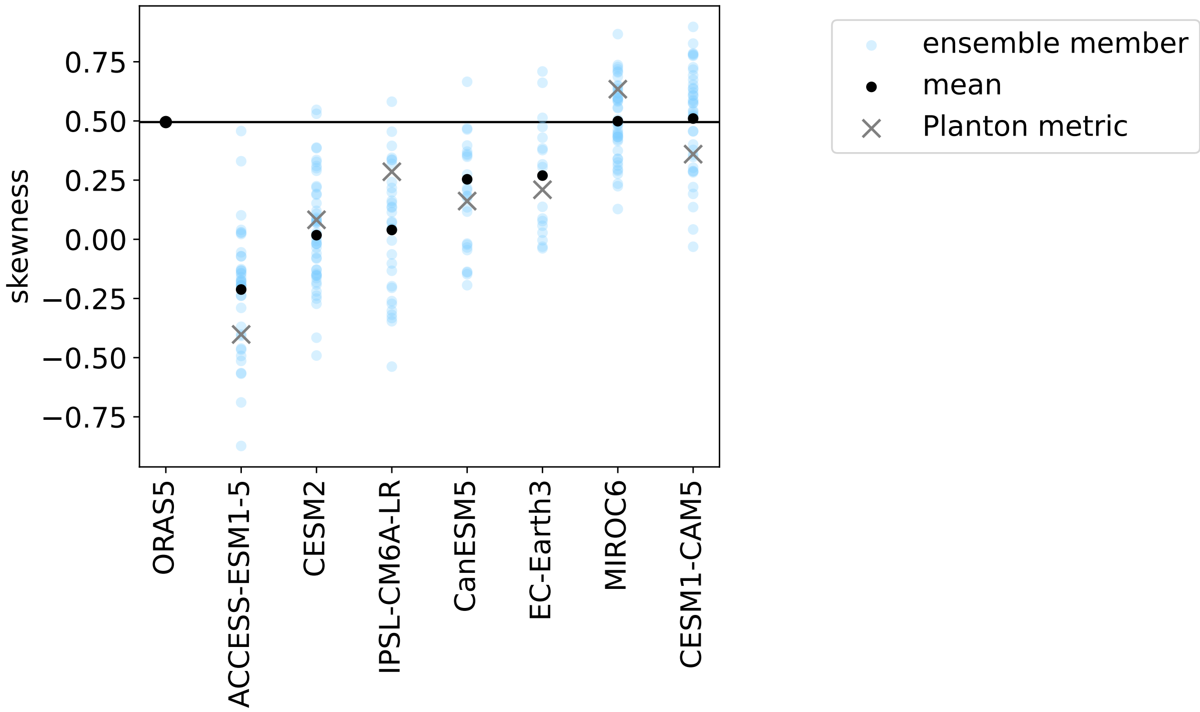


**Figure A1.** Skewness of a 40 year period of each ensemble member, chosen to align with the 40 years of observational record used. For comparison, the Planton metric calculation of skewness (Planton et al., 2021) is marked with a cross, and illustrates that the first ensemble member is not necessarily representative of the entire ensemble.

## Appendix B: Effect of correlation on Bjerknes and Wyrtki indices

390 In some situations, using variables for the ROM where $T$ and $h$ are correlated limits the conclusions that can be drawn from analysis (as argued by Izumo et al., 2019; Dommenget et al., 2023). For analysis through the Bjerknes and Wyrtki indices, as in this work, this constraint does not apply. These indices are the real and imaginary component of the eigenvalues of the linear propagation matrix, thus they are unaffected if one variable is a linear combination of its “true" self and the other. This is a general property of eigenvalues, but is also proven below.

395 Suppose we start with a ROM of the following form (ommitting noise for simplicity):

$$\frac{dT}{dt} = RT + F_1 h, \tag{B1a}$$
$$\frac{dh}{dt} = -\varepsilon h - F_2 T. \tag{B1b}$$

The characteristic equation of the propagation matrix is given by:

$$\lambda^2 + \lambda(\varepsilon - R) + F_1 F_2 - \varepsilon R = 0. \tag{B2}$$

https://doi.org/10.5194/egusphere-2026-5278
Preprint. Discussion started: 22 September 2026


The real and imaginary components of the solutions to this equation (the eigenvalue of the propagation matrix) give the Bjerknes and Wyrtki indices as follows:

$$\text{Bjerknes index} = \mathfrak{Re}(\lambda) = \frac{R-\varepsilon}{2}, \tag{B3a}$$

$$\text{Wyrtki index} = \mathfrak{Im}(\lambda) = \frac{1}{2}\sqrt{4F_1F_2-(R+\varepsilon)^2}, \tag{B3b}$$

Consider instead, for instance, we define a new thermocline variable, $h_n$, which is a linear combination of the original $h$ and $T$. This can be expressed as $h_n = \alpha h + \beta T$ for any $\alpha, \beta \in \mathbb{R}$. The estimated ROM formulation with this new thermocline variable will have the following form:

$$\frac{dT}{dt} = \left(R - \frac{\beta F_1}{\alpha}\right)T + \frac{F_1}{\alpha}h_n, \tag{B4a}$$

$$\frac{dh}{dt} = \left(\frac{\beta F_1}{\alpha} - \varepsilon\right)h_n + \left(\beta R + \beta\varepsilon - \alpha F_2 - \frac{\beta^2 F_1}{\alpha}\right)T. \tag{B4b}$$

The characteristic equation for eigenvalues $\lambda$ is then given by

$$\left(R - \frac{\beta F_1}{\alpha} - \lambda\right)\left(\frac{\beta F_1}{\alpha} - \varepsilon - \lambda\right) - \frac{F_1}{\alpha}\left(\beta R + \beta\varepsilon - \alpha F_2 - \frac{\beta^2 F_1}{\alpha}\right) = 0. \tag{B5}$$

This simplifies to

$$\lambda^2 + \lambda(\varepsilon - R) + F_1F_2 - \varepsilon R = 0. \tag{B6}$$

which is equivalent to the characteristic equation in system (B2), and will give the same eigenvalues and Bjerknes/Wyrtki indices.

Therefore, if one of the $T$ or $h$ variables contains a linear component of the other, this has no impact on the calculation of the Bjerknes and Wyrtki indices, so orthogonality of chosen observational indices does not impact our methodology.

## Appendix C: Fitting and integration of ROM

The $T$ and $h$ we use are monthly averages, rather than instantaneous snapshots. Conceptually, we argue that using these monthly averages to calculate an instantaneous derivative, for the purposes of either fitting or integrating the ROM, does not align with the temporal resolution of data being used. Integrating with a smaller timestep than monthly, or estimating the derivative with a centred difference method, would assume the tendencies are instantaneous. In our use-case, we interpret the tendencies defined by the ROM are as the difference between one month and the next, rather than tan instantaneous derivative as per an ODE in its purest sense. This interpretation is consistent across both the fitting and integration process.

We integrate the ROM with a Euler-Maruyama method with a one-month timestep. In other words, we calculate the tendency of $T$ and $h$ from these variables in any given month, and add this tendency to the values of those variables. We then add independent instances of Gaussian noise to each of $T$ and $h$. This integration approach is paired with the way we fit the ROM, using a least-squares linear regression to estimate the four ROM parameters and then using the standard deviation of the residuals to calculate the amplitude of noise.

https://doi.org/10.5194/egusphere-2026-5278
Preprint. Discussion started: 22 September 2026


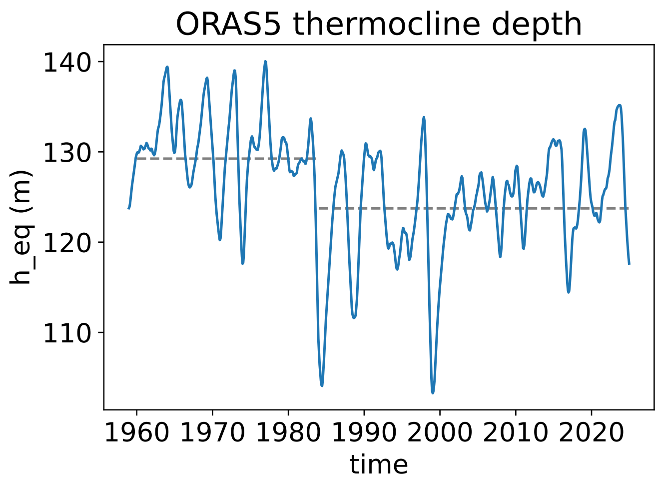


**Figure D1.** Equatorial averaged thermocline depth in ORAS5 demonstrates a step change around 1984, when the first mooring was present in the equatorial Pacific (McPhaden, 1993). We use ORAS5 data from after 1984.

The single-step integration and single-step solve are together much faster and produce a more numerically stable estimate of parameters than using a more complex method, such as a Runge-Kutta solver with a timestep that adjusts (e.g. `scipy.integrate.solve_ivp` default), but which isn't inherently differentiable and therefore necessitates an iterative optimisation (e.g. `scipy.minimize`). When using this iterative solver necessitated by a complex integration method, we found large differences in Bjerknes and Wyrtki indices from small variations in input data. Conversely, the least squares optimisation of the simpler integration method (Euler-Maruayama with one-month timestep, or difference between months) does not have this problem. When paired together, fitting and integrating the ROM both with a one-month timestep means that fitting to an integrated timeseries produces the same parameters used to produce that timeseries within a reasonable error. This is an advantage over integrating with a daily timestep from parameters fitted to monthly differences (empirically verified, but this problem was also highlighted by Weeks and Tziperman (2025)).

**Appendix D: Additional figures**

https://doi.org/10.5194/egusphere-2026-5278
Preprint. Discussion started: 22 September 2026


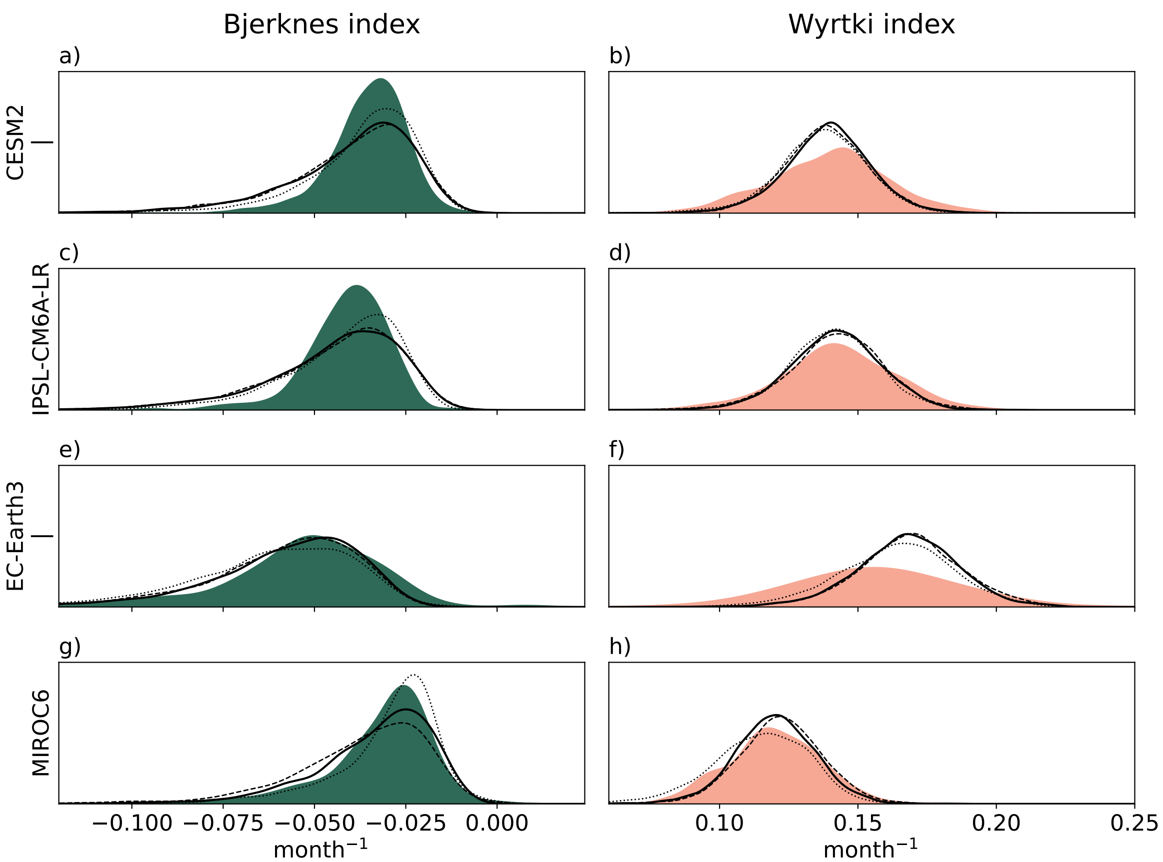


**Figure D2.** As per Fig 3, but repeated for other models. The majority of the EC-Earth3 Wyrtki index discrepancy appears to be from a changing periodicity under climate change (not shown).

https://doi.org/10.5194/egusphere-2026-5278
Preprint. Discussion started: 22 September 2026


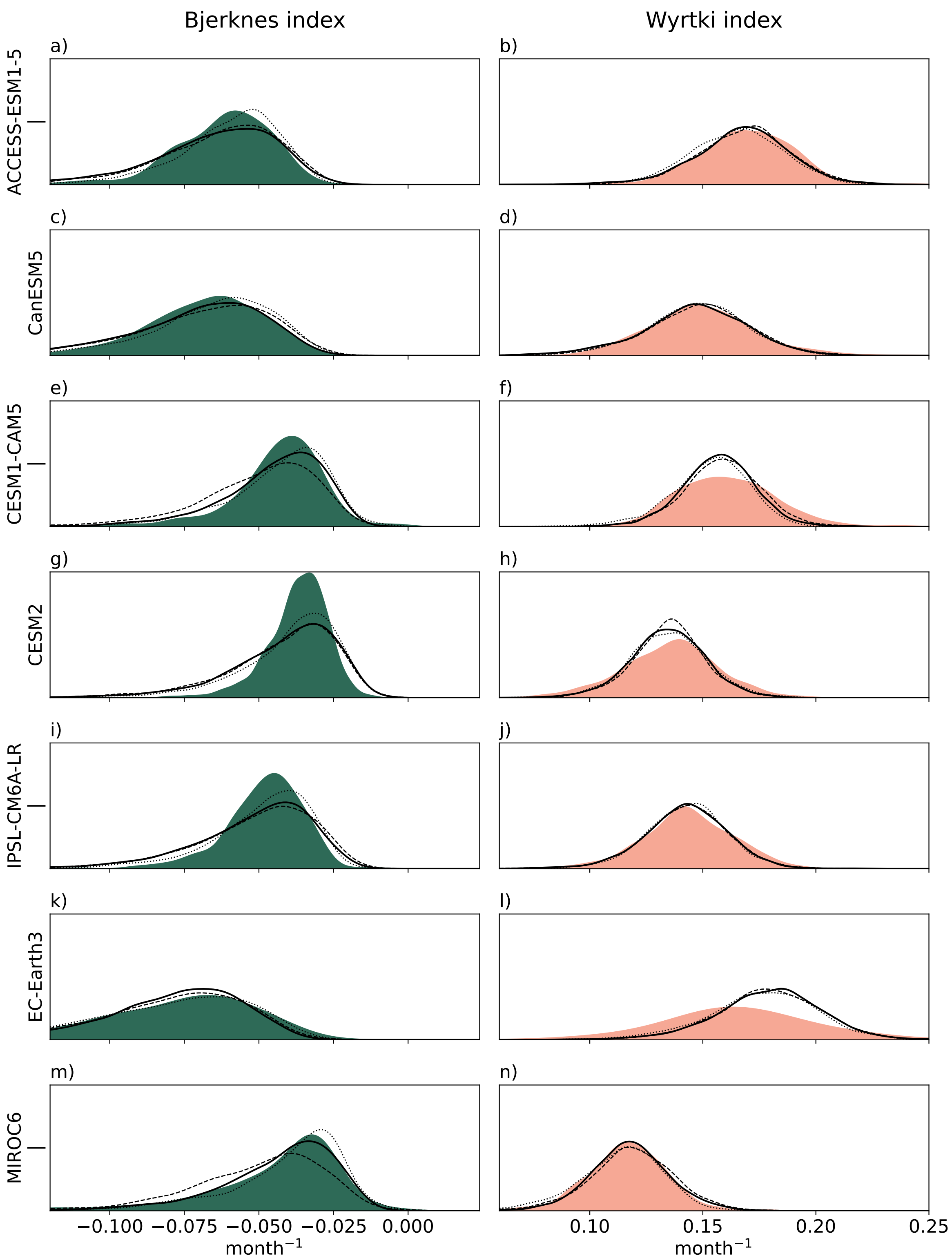


**Figure D3.** As per Fig 3, but using NINO3 instead of NINO34.

https://doi.org/10.5194/egusphere-2026-5278
Preprint. Discussion started: 22 September 2026


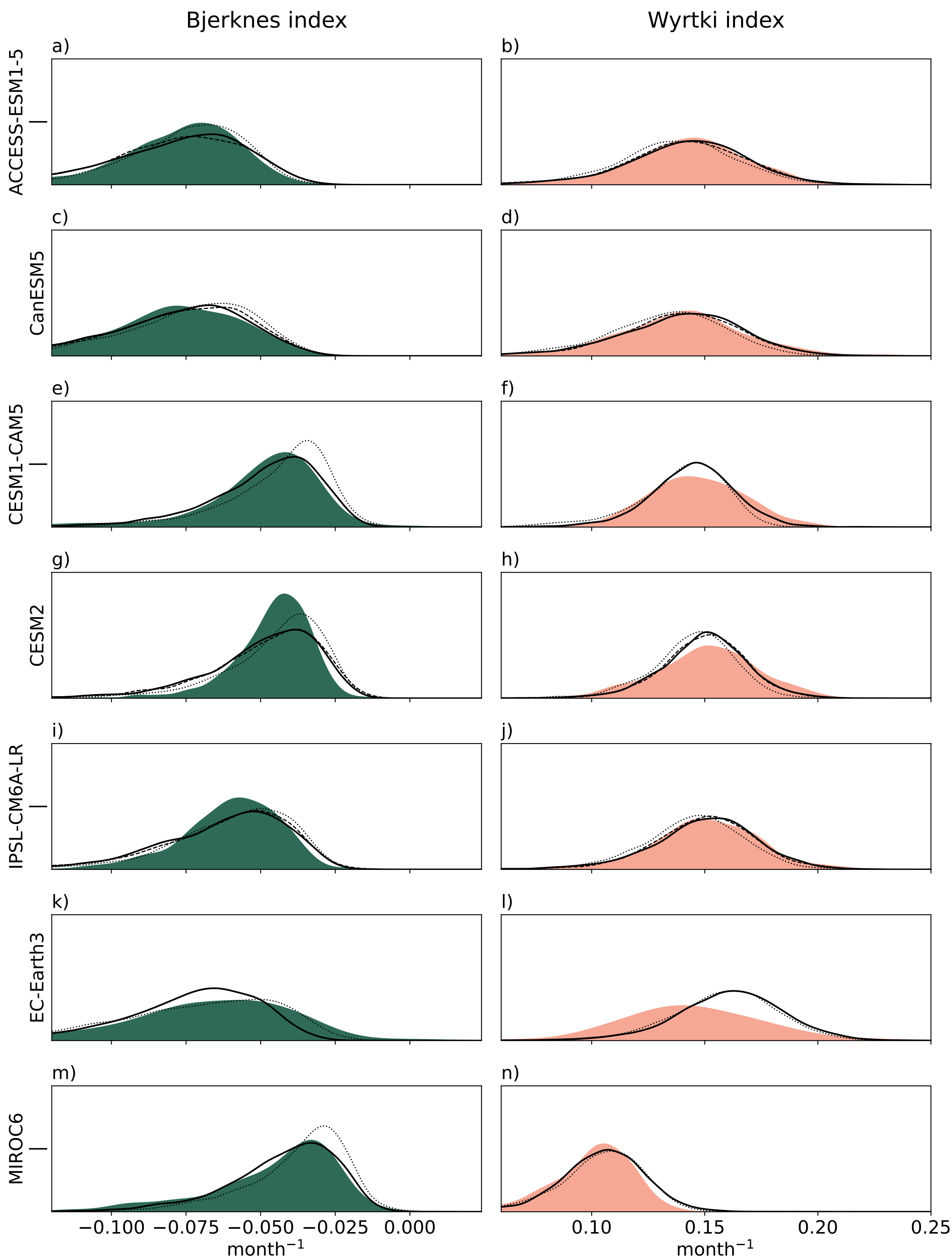




**Figure D4.** As per Fig 3, but using west pacific thermocline depth (120°-205° E) instead of whole equatorial Pacific thermocline depth for $h$. EC-Earth is missing a quadratic ROM because this became unstable.

https://doi.org/10.5194/egusphere-2026-5278
Preprint. Discussion started: 22 September 2026


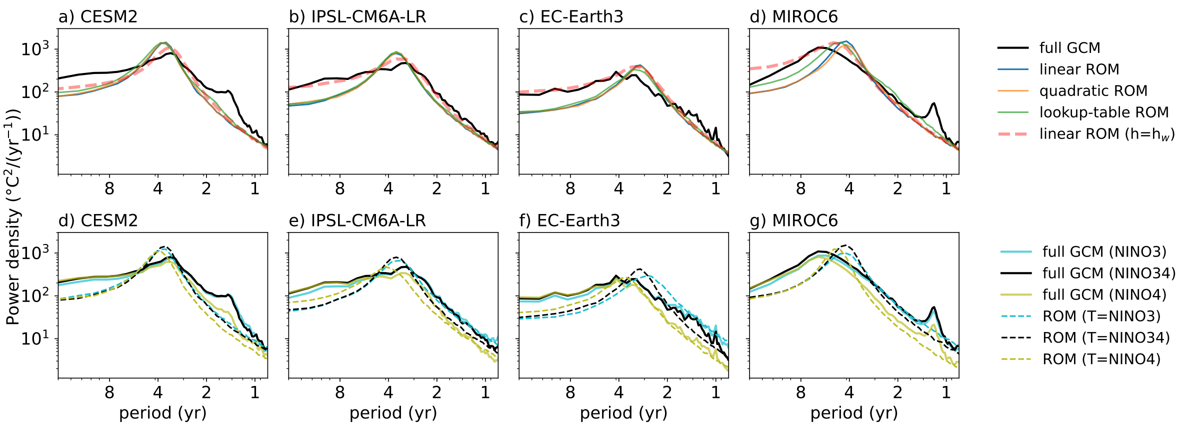


**Figure D5.** As per Fig 4, but repeated for other models

https://doi.org/10.5194/egusphere-2026-5278
Preprint. Discussion started: 22 September 2026


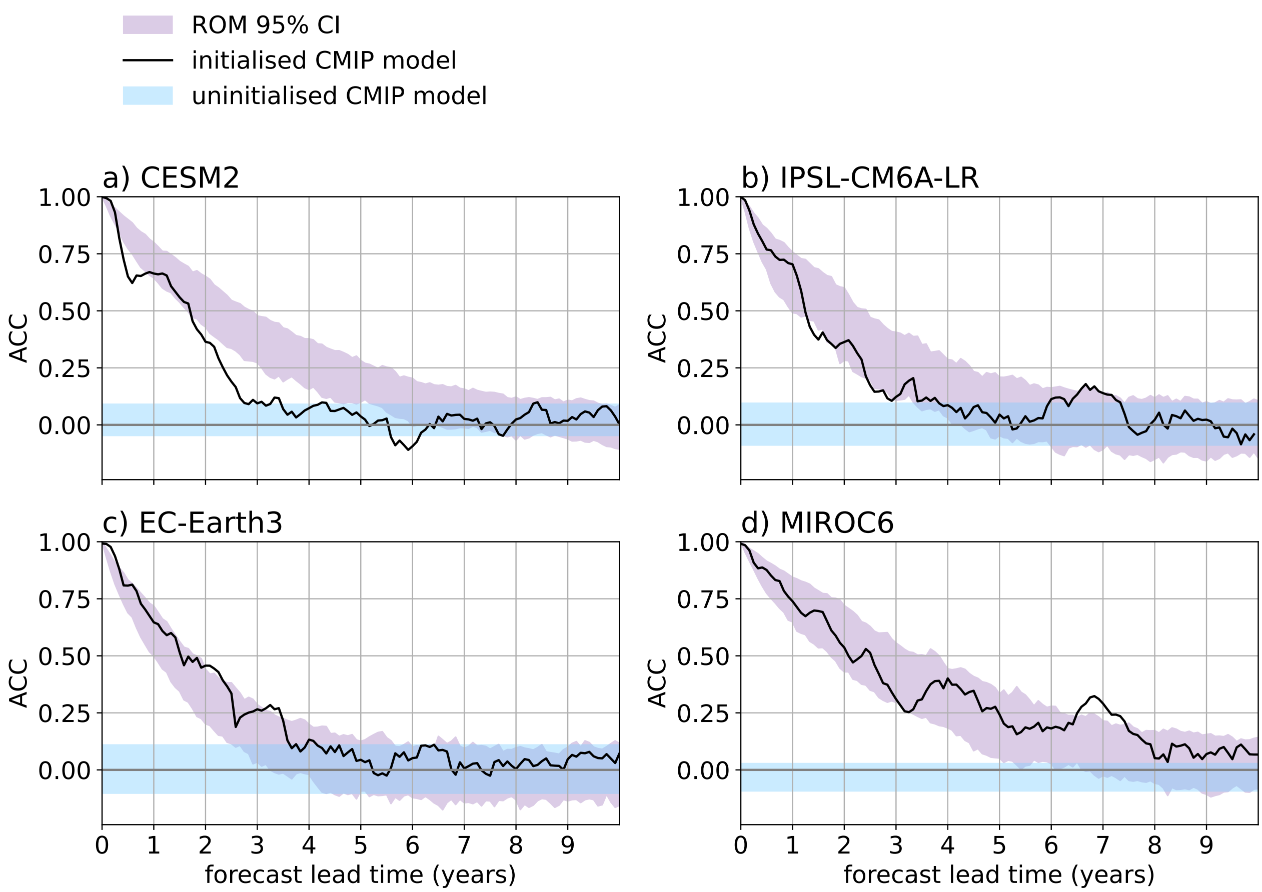


**Figure D6.** As per Fig 5, but repeated for other models. These models have fewer ensemble members (20, 10, 10, 10 for panels a,b,c,d) and show more variation, but still don't show longer timescales of predictability than the ROM.

https://doi.org/10.5194/egusphere-2026-5278
Preprint. Discussion started: 22 September 2026


*Author contributions.* Conceptualization: JJ, CQ; Methodology: JJ, CQ; Data Curation: JJ, NM; Formal analysis and investigation: JJ, CQ; Writing - original draft preparation: JJ, NM; Writing - review and editing: JJ, NM, CQ, DD ; Supervision: NM, CQ, DD

*Competing interests.* The authors have no competing interests to declare

*Acknowledgements.* This research was undertaken with computing resources and support from the Australian National Computational Infrastructure (NCI), which is supported by the Australian Government, and NCAR's Computational and Information Systems Laboratory, sponsored by the National Science Foundation. This research included results using ACCESS-NRI's model ACCESS-ESM1-5 infrastructure, which is enabled by the Australian Government's National Collaborative Research Infrastructure Strategy (NCRIS).

A large language model (Claude AI) was used to review some paragraphs of the manuscript.

JJ and NM were supported by Australian Research Council grant no. DE230100315. CQ was supported by the Australian Research Council grant no. DE250101025. This work originated from work supported by an ARC Centre of Excellence in Climate Extremes Undergraduate Scholarship.

JJ would like to thank Jérôme Vialard for his interest and discussions about this work at EGU24 and subsequent conferences. Without this interest, I wouldn't have had the confidence or motivation to bring these results to a wider audience.

https://doi.org/10.5194/egusphere-2026-5278
Preprint. Discussion started: 22 September 2026


## References

Atwood, A. R., Battisti, D. S., Wittenberg, A. T., Roberts, W. H. G., and Vimont, D. J.: Characterizing unforced multi-decadal variability of ENSO: a case study with the GFDL CM2.1 coupled GCM, Climate Dynamics, 49, 2845–2862, https://doi.org/10.1007/s00382-016-3477-9, 2017.

Barnston, A. G., Tippett, M. K., L'Heureux, M. L., Li, S., and DeWitt, D. G.: Skill of Real-Time Seasonal ENSO Model Predictions during 2002–11: Is Our Capability Increasing?, Bulletin of the American Meteorological Society, 93, 631 – 651, https://doi.org/10.1175/BAMS-D-11-00111.1, 2012.

Bilbao, R., Wild, S., Ortega, P., Acosta-Navarro, J., Arsouze, T., Bretonnière, P.-A., Caron, L.-P., Castrillo, M., Cruz-García, R., Cvijanovic, I., Doblas-Reyes, F. J., Donat, M., Dutra, E., Echevarría, P., Ho, A.-C., Loosveldt-Tomas, S., Moreno-Chamarro, E., Pérez-Zanon, N., Ramos, A., Ruprich-Robert, Y., Sicardi, V., Tourigny, E., and Vegas-Regidor, J.: Assessment of a full-field initialized decadal climate prediction system with the CMIP6 version of EC-Earth, Earth System Dynamics, 12, 173–196, https://doi.org/10.5194/esd-12-173-2021, 2021.

Boer, G. J., Smith, D. M., Cassou, C., Doblas-Reyes, F., Danabasoglu, G., Kirtman, B., Kushnir, Y., Kimoto, M., Meehl, G. A., Msadek, R., Mueller, W. A., Taylor, K. E., Zwiers, F., Rixen, M., Ruprich-Robert, Y., and Eade, R.: The Decadal Climate Prediction Project (DCPP) contribution to CMIP6, Geoscientific Model Development, 9, 3751–3777, https://doi.org/10.5194/gmd-9-3751-2016, 2016.

Borlace, S., Cai, W., and Santoso, A.: Multidecadal ENSO Amplitude Variability in a 1000-yr Simulation of a Coupled Global Climate Model: Implications for Observed ENSO Variability, Journal of Climate, 26, 9399 – 9407, https://doi.org/https://doi.org/10.1175/JCLI-D-13-00281.1, 2013.

Boucher, O., Servonnat, J., Albright, A. L., Aumont, O., Balkanski, Y., Bastrikov, V., Bekki, S., Bonnet, R., Bony, S., Bopp, L., Braconnot, P., Brockmann, P., Cadule, P., Caubel, A., Cheruy, F., Codron, F., Cozic, A., Cugnet, D., D'Andrea, F., Davini, P., de Lavergne, C., Denvil, S., Deshayes, J., Devilliers, M., Ducharne, A., Dufresne, J.-L., Dupont, E., Éthé, C., Fairhead, L., Falletti, L., Flavoni, S., Foujols, M.-A., Gardoll, S., Gastineau, G., Ghattas, J., Grandpeix, J.-Y., Guenet, B., Guez, Lionel, E., Guilyardi, E., Guimberteau, M., Hauglustaine, D., Hourdin, F., Idelkadi, A., Joussaume, S., Kageyama, M., Khodri, M., Krinner, G., Lebas, N., Levavasseur, G., Lévy, C., Li, L., Lott, F., Lurton, T., Luyssaert, S., Madec, G., Madeleine, J.-B., Maignan, F., Marchand, M., Marti, O., Mellul, L., Meurdesoif, Y., Mignot, J., Musat, I., Ottlé, C., Peylin, P., Planton, Y., Polcher, J., Rio, C., Rochetin, N., Rousset, C., Sepulchre, P., Sima, A., Swingedouw, D., Thiéblemont, R., Traore, A. K., Vancoppenolle, M., Vial, J., Vialard, J., Viovy, N., and Vuichard, N.: Presentation and Evaluation of the IPSL-CM6A-LR Climate Model, Journal of Advances in Modeling Earth Systems, 12, e2019MS002 010, https://doi.org/https://doi.org/10.1029/2019MS002010, e2019MS002010 10.1029/2019MS002010, 2020.

Burgman, R. J., Schopf, P. S., and Kirtman, B. P.: Decadal Modulation of ENSO in a Hybrid Coupled Model, Journal of Climate, 21, 5482 – 5500, https://doi.org/https://doi.org/10.1175/2008JCLI1933.1, 2008.

Capotondi, A. and Sardeshmukh, P. D.: Is El Niño really changing?, Geophysical Research Letters, 44, 8548–8556, https://doi.org/https://doi.org/10.1002/2017GL074515, 2017.

Capotondi, A., Sardeshmukh, P. D., and Ricciardulli, L.: The Nature of the Stochastic Wind Forcing of ENSO, Journal of Climate, 31, 8081 – 8099, https://doi.org/10.1175/JCLI-D-17-0842.1, 2018.

Capotondi, A., McGregor, S., McPhaden, M. J., Cravatte, S., Holbrook, N. J., Imada, Y., Sanchez, S. C., Sprintall, J., Stuecker, M. F., Ummenhofer, C. C., Zeller, M., Farneti, R., Graffino, G., Hu, S., Karnauskas, K. B., Kosaka, Y., Kucharski, F., Mayer, M., Qiu, B., Santoso, A., Taschetto, A. S., Wang, F., Zhang, X., Holmes, R. M., Luo, J.-J., Maher, N., Martinez-Villalobos, C., Meehl, G. A., Naha, R.,

https://doi.org/10.5194/egusphere-2026-5278
Preprint. Discussion started: 22 September 2026


Schneider, N., Stevenson, S., Sullivan, A., van Rensch, P., and Xu, T.: Mechanisms of tropical Pacific decadal variability, Nature Reviews Earth & Environment, https://doi.org/10.1038/s43017-023-00486-x, 2023.

Chen, H.-C. and Jin, F.-F.: Fundamental Behavior of ENSO Phase Locking, Journal of Climate, 33, 1953 – 1968, https://doi.org/10.1175/JCLI-D-19-0264.1, 2020.

Chen, H.-C. and Jin, F.-F.: Simulations of ENSO Phase-Locking in CMIP5 and CMIP6, Journal of Climate, 34, 5135 – 5149, https://doi.org/10.1175/JCLI-D-20-0874.1, 2021.

Chen, N., Fang, X., and Yu, J.-Y.: A multiscale model for El Niño complexity, npj Climate and Atmospheric Science, 5, 16, https://doi.org/10.1038/s41612-022-00241-x, 2022.

Choi, J., An, S.-I., and Yeh, S.-W.: Decadal amplitude modulation of two types of ENSO and its relationship with the mean state, Climate Dynamics, 38, 2631–2644, https://doi.org/10.1007/s00382-011-1186-y, 2012.

Copernicus Climate Change Service, C. D. S.: ORAS5 global ocean reanalysis monthly data from 1958 to present, online dataset, https://doi.org/https://doi.org/10.24381/cds.67e8eeb7, 2021.

Crespo, L. R., Belén Rodríguez-Fonseca, M., Polo, I., Keenlyside, N., and Dommenget, D.: Multidecadal variability of ENSO in a recharge oscillator framework, Environmental Research Letters, 17, 074 008, https://doi.org/10.1088/1748-9326/ac72a3, 2022.

Dieppois, B., Capotondi, A., Pohl, B., Chun, K. P., Monerie, P.-A., and Eden, J.: ENSO diversity shows robust decadal variations that must be captured for accurate future projections, Communications Earth & Environment, 2, 212, https://doi.org/10.1038/s43247-021-00285-6, 2021.

Dommenget, D. and Al-Ansari, M.: Asymmetries in the ENSO phase space, Climate Dynamics, 60, 2147–2166, https://doi.org/10.1007/s00382-022-06392-0, 2023.

Dommenget, D., Priya, P., and Vijayeta, A.: ENSO phase space dynamics with an improved estimate of the thermocline depth, Climate Dynamics, 61, 5767–5783, https://doi.org/10.1007/s00382-023-06883-8, 2023.

Döscher, R., Acosta, M., Alessandri, A., Anthoni, P., Arsouze, T., Bergman, T., Bernardello, R., Boussetta, S., Caron, L.-P., Carver, G., Castrillo, M., Catalano, F., Cvijanovic, I., Davini, P., Dekker, E., Doblas-Reyes, F. J., Docquier, D., Echevarria, P., Fladrich, U., Fuentes-Franco, R., Gröger, M., v. Hardenberg, J., Hieronymus, J., Karami, M. P., Keskinen, J.-P., Koenigk, T., Makkonen, R., Massonnet, F., Ménégoz, M., Miller, P. A., Moreno-Chamarro, E., Nieradzik, L., van Noije, T., Nolan, P., O'Donnell, D., Ollinaho, P., van den Oord, G., Ortega, P., Prims, O. T., Ramos, A., Reerink, T., Rousset, C., Ruprich-Robert, Y., Le Sager, P., Schmith, T., Schrödner, R., Serva, F., Sicardi, V., Sloth Madsen, M., Smith, B., Tian, T., Tourigny, E., Uotila, P., Vancoppenolle, M., Wang, S., Wårlind, D., Willén, U., Wyser, K., Yang, S., Yepes-Arbós, X., and Zhang, Q.: The EC-Earth3 Earth system model for the Coupled Model Intercomparison Project 6, Geoscientific Model Development, 15, 2973–3020, https://doi.org/10.5194/gmd-15-2973-2022, 2022.

Fang, X.-H., Zheng, F., Liu, Z.-Y., and Zhu, J.: Decadal Modulation of ENSO Spring Persistence Barrier by Thermal Damping Processes in the Observation, Geophysical Research Letters, 46, 6892–6899, https://doi.org/https://doi.org/10.1029/2019GL082921, 2019.

Fedorov, A. V., Hu, S., Wittenberg, A. T., Levine, A. F. Z., and Deser, C.: ENSO Low-Frequency Modulation and Mean State Interactions, chap. 8, pp. 173–198, American Geophysical Union (AGU), ISBN 9781119548164, https://doi.org/https://doi.org/10.1002/9781119548164.ch8, 2020.

Feng, Y. and Tung, K.-K.: ENSO modulation: real and apparent; implications for decadal prediction, Climate Dynamics, 54, 615–629, https://doi.org/10.1007/s00382-019-05016-4, 2020.

Gong, Y., Li, T., and Chen, L.: Interdecadal modulation of ENSO amplitude by the Atlantic multi-decadal oscillation (AMO), Climate Dynamics, 55, 2689–2702, https://doi.org/10.1007/s00382-020-05408-x, 2020.

Han, S., Fedorov, A. V., and Vialard, J.: Realistic ENSO Dynamics Requires a Damped Nonlinear Recharge Oscillator, Journal of Climate, 39, 77 – 101, https://doi.org/10.1175/JCLI-D-25-0250.1, 2026.

Han, S., Vialard, J., Fedorov, A. V., and Kim, S.-K.: Internal Variability Limits Detection of Forced ENSO Changes: Insights From the Recharge Oscillator, Geophysical Research Letters, under review.

Harris, C. R., Millman, K. J., van der Walt, S. J., Gommers, R., Virtanen, P., Cournapeau, D., Wieser, E., Taylor, J., Berg, S., Smith, N. J., Kern, R., Picus, M., Hoyer, S., van Kerkwijk, M. H., Brett, M., Haldane, A., del Río, J. F., Wiebe, M., Peterson, P., Gérard-Marchant, P., Sheppard, K., Reddy, T., Weckesser, W., Abbasi, H., Gohlke, C., and Oliphant, T. E.: Array programming with NumPy, Nature, 585, 357–362, https://doi.org/10.1038/s41586-020-2649-2, 2020.

Henley, B. J., Meehl, G., Power, S. B., Folland, C. K., King, A. D., Brown, J. N., Karoly, D. J., Delage, F., Gallant, A. J. E., Freund, M., and Neukom, R.: Spatial and temporal agreement in climate model simulations of the Interdecadal Pacific Oscillation, Environmental Research Letters, 12, 044 011, https://doi.org/10.1088/1748-9326/aa5cc8, 2017.

Hoyer, S. and Hamman, J.: xarray: N-D labeled arrays and datasets in Python, In revision, J. Open Res. Software, 2017.

Hu, Z.-Z., Kumar, A., Huang, B., Zhu, J., LHeureux, M., McPhaden, M., and Yu, J.-Y.: The Interdecadal Shift of ENSO Properties in 1999/2000: A Review, Journal of Climate, 33, 4441–4462, https://doi.org/10.1175/JCLI-D-19-0316.1, 2020.

Hunter, J. D.: Matplotlib: A 2D graphics environment, Computing in Science & Engineering, 9, 90–95, https://doi.org/10.1109/MCSE.2007.55, 2007.

Imada, Y. and Kimoto, M.: ENSO amplitude modulation related to Pacific decadal variability, Geophysical Research Letters, 36, https://doi.org/10.1029/2008GL036421, 2009.

Izumo, T., Lengaigne, M., Vialard, J., Suresh, I., and Planton, Y.: On the physical interpretation of the lead relation between Warm Water Volume and the El Niño Southern Oscillation, Climate Dynamics, 52, 2923–2942, https://doi.org/10.1007/s00382-018-4313-1, 2019.

Jansen, M. F., Dommenget, D., and Keenlyside, N.: Tropical Atmosphere–Ocean Interactions in a Conceptual Framework, Journal of Climate, 22, 550 – 567, https://doi.org/10.1175/2008JCLI2243.1, 2009.

Jin, F.: An Equatorial Ocean Recharge Paradigm for ENSO. Part I: Conceptual Model, Journal of the Atmospheric Sciences, 54, 811–829, 1997.

Jin, F.-F., Kim, S. T., and Bejarano, L.: A coupled-stability index for ENSO, Geophysical Research Letters, 33, https://doi.org/https://doi.org/10.1029/2006GL027221, 2006.

Jin, F.-F., Lin, L., Timmermann, A., and Zhao, J.: Ensemble-mean dynamics of the ENSO recharge oscillator under state-dependent stochastic forcing, Geophysical Research Letters, 34, https://doi.org/https://doi.org/10.1029/2006GL027372, 2007.

Jin, F.-F., Chen, H.-C., Zhao, S., Hayashi, M., Karamperidou, C., Stuecker, M. F., Xie, R., and Geng, L.: Simple ENSO Models, chap. 6, pp. 119–151, American Geophysical Union (AGU), ISBN 9781119548164, https://doi.org/https://doi.org/10.1002/9781119548164.ch6, 2020.

Kataoka, T., Tatebe, H., Koyama, H., Mochizuki, T., Ogochi, K., Naoe, H., Imada, Y., Shiogama, H., Kimoto, M., and Watanabe, M.: Seasonal to Decadal Predictions With MIROC6: Description and Basic Evaluation, Journal of Advances in Modeling Earth Systems, 12, e2019MS002 035, https://doi.org/https://doi.org/10.1029/2019MS002035, e2019MS002035 2019MS002035, 2020.

Kay, J. E., Deser, C., Phillips, A., Mai, A., Hannay, C., Strand, G., Arblaster, J. M., Bates, S. C., Danabasoglu, G., Edwards, J., Holland, M., Kushner, P., Lamarque, J.-F., Lawrence, D., Lindsay, K., Middleton, A., Munoz, E., Neale, R., Oleson, K., Polvani, L., and Vertenstein, M.: The Community Earth System Model (CESM) Large Ensemble Project: A Community Resource for Studying Climate Change in the Presence of Internal Climate Variability, Bulletin of the American Meteorological Society, 96, 1333 – 1349, https://doi.org/10.1175/BAMS-D-13-00255.1, 2015.

Kim, G.-I. and Kug, J.-S.: Process-Based Analysis of El Niño–Southern Oscillation Decadal Modulation, Journal of Climate, 35, 4753 – 4769, https://doi.org/https://doi.org/10.1175/JCLI-D-21-0181.1, 2022.

Kim, S.-K. and An, S.-I.: Untangling El Niño-La Niña Asymmetries Using a Nonlinear Coupled Dynamic Index, Geophysical Research Letters, 47, e2019GL085 881, https://doi.org/https://doi.org/10.1029/2019GL085881, e2019GL085881 2019GL085881, 2020.

Kohyama, T., Hartmann, D. L., and Battisti, D. S.: La Niña–like Mean-State Response to Global Warming and Potential Oceanic Roles, Journal of Climate, 30, 4207 – 4225, https://doi.org/10.1175/JCLI-D-16-0441.1, 2017.

Levine, A., Jin, F. F., and McPhaden, M. J.: Extreme Noise–Extreme El Niño: How State-Dependent Noise Forcing Creates El Niño–La Niña Asymmetry, Journal of Climate, 29, 5483 – 5499, https://doi.org/10.1175/JCLI-D-16-0091.1, 2016.

Levine, A. F. Z. and McPhaden, M. J.: The annual cycle in ENSO growth rate as a cause of the spring predictability barrier, Geophysical Research Letters, 42, 5034–5041, https://doi.org/https://doi.org/10.1002/2015GL064309, 2015.

Lu, B., Jin, F.-F., and Ren, H.-L.: A Coupled Dynamic Index for ENSO Periodicity, Journal of Climate, 31, 2361 – 2376, https://doi.org/10.1175/JCLI-D-17-0466.1, 2018.

Lübbecke, J. and McPhaden, M.: Assessing the Twenty-First-Century Shift in ENSO Variability in Terms of the Bjerknes Stability Index*, Journal of Climate, 27, https://doi.org/10.1175/JCLI-D-13-00438.1, 2014.

Maher, N., Phillips, A. S., Deser, C., Wills, R. C. J., Lehner, F., Fasullo, J., Caron, J. M., Brunner, L., Beyerle, U., and Jeffree, J.: The updated Multi-Model Large Ensemble Archive and the Climate Variability Diagnostics Package: new tools for the study of climate variability and change, Geoscientific Model Development, 18, 6341–6365, https://doi.org/10.5194/gmd-18-6341-2025, 2025.

McPhaden, M. J.: TOGA-TAO and the 1991-93 El Niño-Southern Oscillation Event, Oceanography, 6, 36–44, http://www.jstor.org/stable/43924639, 1993.

McPhaden, M. J.: A 21st century shift in the relationship between ENSO SST and warm water volume anomalies, Geophysical Research Letters, 39, https://doi.org/https://doi.org/10.1029/2012GL051826, 2012.

Newman, M., Shin, S.-I., and Alexander, M. A.: Natural variation in ENSO flavors, Geophysical Research Letters, 38, https://doi.org/https://doi.org/10.1029/2011GL047658, 2011.

Pascolini-Campbell, M., Zanchettin, D., Bothe, O., Timmreck, C., Matei, D., Jungclaus, J. H., and Graf, H. F.: Toward a record of Central Pacific El Niño events since 1880, Theoretical and Applied Climatology, 119, 379–389, https://doi.org/10.1007/s00704-014-1114-2, 2015.

Planton, Y. Y., Guilyardi, E., Wittenberg, A. T., Lee, J., Gleckler, P. J., Bayr, T., McGregor, S., McPhaden, M. J., Power, S., Roehrig, R., Vialard, J., and Voldoire, A.: Evaluating Climate Models with the CLIVAR 2020 ENSO Metrics Package, Bulletin of the American Meteorological Society, 102, E193 – E217, https://doi.org/https://doi.org/10.1175/BAMS-D-19-0337.1, 2021.

Priya, P. and Dommenget, D.: ENSO phase space dynamics in CMIP models, Climate Dynamics, 63, 270, https://doi.org/10.1007/s00382-025-07752-2, 2025.

Ren, H.-L. and Wang, R.: Diagnosing the Linear Periodicity Dynamics of ENSO for Its Two Spatiotemporal Modes, Geophysical Research Letters, 50, e2023GL105 756, https://doi.org/https://doi.org/10.1029/2023GL105756, e2023GL105756 2023GL105756, 2023.

Ren, Z. and Zhou, T.: Understanding the alleviation of "Double-ITCZ"bias in CMIP6 models from the perspective of atmospheric energy balance, Climate Dynamics, 62, 6819–6839, https://doi.org/10.1007/s00382-024-07238-7, 2024.

Rodgers, K. B., Lee, S.-S., Rosenbloom, N., Timmermann, A., Danabasoglu, G., Deser, C., Edwards, J., Kim, J.-E., Simpson, I. R., Stein, K., Stuecker, M. F., Yamaguchi, R., Bódai, T., Chung, E.-S., Huang, L., Kim, W. M., Lamarque, J.-F., Lombardozzi, D. L., Wieder, W. R., and Yeager, S. G.: Ubiquity of human-induced changes in climate variability, Earth System Dynamics, 12, 1393–1411, https://doi.org/10.5194/esd-12-1393-2021, 2021.

Schlör, J., Strnad, F., Capotondi, A., and Goswami, B.: Contribution of El Niño Southern Oscillation (ENSO) Diversity to Low-Frequency Changes in ENSO Variance, Geophysical Research Letters, 51, e2024GL109 179, https://doi.org/https://doi.org/10.1029/2024GL109179, e2024GL109179 2024GL109179, 2024.

Sospedra-Alfonso, R., Merryfield, W. J., Boer, G. J., Kharin, V. V., Lee, W.-S., Seiler, C., and Christian, J. R.: Decadal climate predictions with the Canadian Earth System Model version 5 (CanESM5), Geoscientific Model Development, 14, 6863–6891, https://doi.org/10.5194/gmd-14-6863-2021, 2021.

Sun, T. and Okumura, Y.: Impact of ENSO-Like Tropical Pacific Decadal Variability on the Relative Frequency of El Niño and La Niña Events, Geophysical Research Letters, 47, https://doi.org/10.1029/2019GL085832, cited By 2, 2020.

Swart, N. C., Cole, J. N. S., Kharin, V. V., Lazare, M., Scinocca, J. F., Gillett, N. P., Anstey, J., Arora, V., Christian, J. R., Hanna, S., Jiao, Y., Lee, W. G., Majaess, F., Saenko, O. A., Seiler, C., Seinen, C., Shao, A., Sigmond, M., Solheim, L., von Salzen, K., Yang, D., and Winter, B.: The Canadian Earth System Model version 5 (CanESM5.0.3), Geoscientific Model Development, 12, 4823–4873, https://doi.org/10.5194/gmd-12-4823-2019, 2019.

Swingedouw, D., Reiter, R., Mignot, J., Gastineau, G., Torres, O., and Alkama, R.: Evaluation of two versions of the IPSL-EPOC decadal prediction systems, Frontiers in Climate, Volume 8 - 2026, https://doi.org/10.3389/fclim.2026.1803256, 2026.

Takahashi, K., Karamperidou, C., and Dewitte, B.: A theoretical model of strong and moderate El Niño regimes, Climate Dynamics, 52, 7477–7493, https://doi.org/10.1007/s00382-018-4100-z, 2019.

Tatebe, H., Ogura, T., Nitta, T., Komuro, Y., Ogochi, K., Takemura, T., Sudo, K., Sekiguchi, M., Abe, M., Saito, F., Chikira, M., Watanabe, S., Mori, M., Hirota, N., Kawatani, Y., Mochizuki, T., Yoshimura, K., Takata, K., O'ishi, R., Yamazaki, D., Suzuki, T., Kurogi, M., Kataoka, T., Watanabe, M., and Kimoto, M.: Description and basic evaluation of simulated mean state, internal variability, and climate sensitivity in MIROC6, Geoscientific Model Development, 12, 2727–2765, https://doi.org/10.5194/gmd-12-2727-2019, 2019.

Thual, S. and Dewitte, B.: ENSO complexity controlled by zonal shifts in the Walker circulation, Nature Geoscience, 16, 328–332, https://doi.org/10.1038/s41561-023-01154-x, 2023.

Tian, B., Ren, H.-L., Jin, F.-F., and Stuecker, M. F.: Diagnosing the representation and causes of the ENSO persistence barrier in CMIP5 simulations, Climate Dynamics, 53, 2147–2160, https://doi.org/10.1007/s00382-019-04810-4, 2019.

Timmermann, A. and Jin, F.-F.: A Nonlinear Mechanism for Decadal El NiñO Amplitude Changes, Geophysical Research Letters, 29, 3–1–3–4, https://doi.org/https://doi.org/10.1029/2001GL013369, 2002.

Timmermann, A., An, S.-I., Kug, J.-S., Jin, F.-F., Cai, W., Capotondi, A., Cobb, K. M., Lengaigne, M., McPhaden, M. J., Stuecker, M. F., Stein, K., Wittenberg, A. T., Yun, K.-S., Bayr, T., Chen, H.-C., Chikamoto, Y., Dewitte, B., Dommenget, D., Grothe, P., Guilyardi, E., Ham, Y.-G., Hayashi, M., Ineson, S., Kang, D., Kim, S., Kim, W., Lee, J.-Y., Li, T., Luo, J.-J., McGregor, S., Planton, Y., Power, S., Rashid, H., Ren, H.-L., Santoso, A., Takahashi, K., Todd, A., Wang, G., Wang, G., Xie, R., Yang, W.-H., Yeh, S.-W., Yoon, J., Zeller, E., and Zhang, X.: El Niño–Southern Oscillation complexity, Nature, 559, 535–545, https://doi.org/10.1038/s41586-018-0252-6, 2018.

Vialard, J., Jin, F. F., McPhaden, M. J., Fedorov, A., Cai, W., An, S. I., Dommenget, D., Fang, X., Stuecker, M. F., Wang, C., Wittenberg, A., Zhao, S., Liu, F., Kim, S. K., Planton, Y., Geng, T., Lengaigne, M., Capotondi, A., Chen, N., Geng, L., Hu, S., Izumo, T., Kug, J. S., Luo, J. J., McGregor, S., Pagli, B., Priya, P., Stevenson, S., and Thual, S.: The El Niño Southern Oscillation (ENSO) Recharge Oscillator Conceptual Model: Achievements and Future Prospects, Reviews of Geophysics, 63, e2024RG000 843, https://doi.org/https://doi.org/10.1029/2024RG000843, 2025.

Vijayeta, A. and Dommenget, D.: An evaluation of ENSO dynamics in CMIP simulations in the framework of the recharge oscillator model, Climate Dynamics, 51, 1753–1771, https://doi.org/10.1007/s00382-017-3981-6, 2018.

Virtanen, P., Gommers, R., Oliphant, T. E., Haberland, M., Reddy, T., Cournapeau, D., Burovski, E., Peterson, P., Weckesser, W., Bright, J., van der Walt, S. J., Brett, M., Wilson, J., Millman, K. J., Mayorov, N., Nelson, A. R. J., Jones, E., Kern, R., Larson, E., Carey, C. J., Polat, İ., Feng, Y., Moore, E. W., VanderPlas, J., Laxalde, D., Perktold, J., Cimrman, R., Henriksen, I., Quintero, E. A., Harris, C. R., Archibald, A. M., Ribeiro, A. H., Pedregosa, F., van Mulbregt, P., and SciPy 1.0 Contributors: SciPy 1.0: Fundamental Algorithms for Scientific Computing in Python, Nature Methods, 17, 261–272, https://doi.org/10.1038/s41592-019-0686-2, 2020.

Weeks, E. and Tziperman, E.: Challenges in Determining Whether ENSO Is a Damped or a Self-Sustained Oscillation, Geophysical Research Letters, 52, e2025GL116 328, https://doi.org/https://doi.org/10.1029/2025GL116328, e2025GL116328 2025GL116328, 2025.

Weisheimer, A., Balmaseda, M. A., Stockdale, T. N., Mayer, M., Sharmila, S., Hendon, H., and Alves, O.: Variability of ENSO forecast skill in 2-year global reforecasts over the 20th Century, Geophysical Research Letters, n/a, e2022GL097 885, https://doi.org/https://doi.org/10.1029/2022GL097885, e2022GL097885 2022GL097885, 2022.

Williams, I. N. and Patricola, C. M.: Diversity of ENSO Events Unified by Convective Threshold Sea Surface Temperature: A Nonlinear ENSO Index, Geophysical Research Letters, 45, 9236–9244, https://doi.org/https://doi.org/10.1029/2018GL079203, 2018.

Wittenberg, A., Rosati, A., Delworth, T., Vecchi, G., and Zeng, F.: ENSO modulation: Is it decadally predictable?, Journal of Climate, 27, 2667–2681, https://doi.org/10.1175/JCLI-D-13-00577.1, 2014.

Wyser, K., Koenigk, T., Fladrich, U., Fuentes-Franco, R., Karami, M. P., and Kruschke, T.: The SMHI Large Ensemble (SMHI-LENS) with EC-Earth3.3.1, Geoscientific Model Development, 14, 4781–4796, https://doi.org/10.5194/gmd-14-4781-2021, 2021.

Yeager, S. G., Danabasoglu, G., Rosenbloom, N. A., Strand, W., Bates, S. C., Meehl, G. A., Karspeck, A. R., Lindsay, K., Long, M. C., Teng, H., and Lovenduski, N. S.: Predicting Near-Term Changes in the Earth System: A Large Ensemble of Initialized Decadal Prediction Simulations Using the Community Earth System Model, Bulletin of the American Meteorological Society, 99, 1867 – 1886, https://doi.org/10.1175/BAMS-D-17-0098.1, 2018.

Yeager, S. G., Rosenbloom, N., Glanville, A. A., Wu, X., Simpson, I., Li, H., Molina, M. J., Krumhardt, K., Mogen, S., Lindsay, K., Lombardozzi, D., Wieder, W., Kim, W. M., Richter, J. H., Long, M., Danabasoglu, G., Bailey, D., Holland, M., Lovenduski, N., Strand, W. G., and King, T.: The Seasonal-to-Multiyear Large Ensemble (SMYLE) prediction system using the Community Earth System Model version 2, Geoscientific Model Development, 15, 6451–6493, https://doi.org/10.5194/gmd-15-6451-2022, 2022.

Zeller, M., McGregor, S., van Sebille, E., Capotondi, A., and Spence, P.: Subtropical-tropical pathways of spiciness anomalies and their impact on equatorial Pacific temperature, Climate Dynamics, 56, 1131–1144, https://doi.org/10.1007/s00382-020-05524-8, 2021.

Zhao, S., Jin, F.-F., Stuecker, M. F., Thompson, P. R., Kug, J.-S., McPhaden, M. J., Cane, M. A., Wittenberg, A. T., and Cai, W.: Explainable El Niño predictability from climate mode interactions, Nature, 630, 891–898, https://doi.org/10.1038/s41586-024-07534-6, 2024.

Zheng, F., Fang, X. H., Zhu, J., Yu, J. Y., and Li, X. C.: Modulation of Bjerknes feedback on the decadal variations in ENSO predictability, Geophysical Research Letters, 43, 12,560–12,568, https://doi.org/10.1002/2016GL071636, 2016.

Ziehn, T., Chamberlain, M. A., Law, R. M., Lenton, A., Bodman, R. W., Dix, M., Stevens, L., Wang, Y.-P., and Srbinovsky, J.: The Australian Earth System Model: ACCESS-ESM1.5, Journal of Southern Hemisphere Earth Systems Science, 70, 193–214, https://doi.org/10.1071/ES19035, 2020.